The Plant Cell, Vol. 25: 1523–1540, May 2013, www.plantcell.org

LARGE-SCALE BIOLOGY ARTICLE

Advanced Proteomic Analyses Yield a Deep Catalog of Ubiquitylation Targets in *Arabidopsis*[W]

Do-Young Kim,[a] Mark Scalf,[b] Lloyd M. Smith,[b] and Richard D. Vierstra[a,1]

[a] Department of Genetics, University of Wisconsin, Madison, Wisconsin 53706
[b] Department of Chemistry,University of Wisconsin, Madison, Wisconsin 53706

The posttranslational addition of ubiquitin (Ub) profoundly controls the half-life, interactions, and/or trafficking of numerous intracellular proteins. Using stringent two-step affinity methods to purify Ub-protein conjugates followed by high-sensitivity mass spectrometry, we identified almost 950 ubiquitylation substrates in whole *Arabidopsis thaliana* seedlings. The list includes key factors regulating a wide range of biological processes, including metabolism, cellular transport, signal transduction, transcription, RNA biology, translation, and proteolysis. The ubiquitylation state of more than half of the targets increased after treating seedlings with the proteasome inhibitor MG132 (carbobenzoxy-Leu-Leu-Leu-al), strongly suggesting that Ub addition commits many to degradation by the 26S proteasome. Ub-attachment sites were resolved for a number of targets, including six of the seven Lys residues on Ub itself with a Lys-48>Lys-63>Lys-11>>>Lys-33/Lys-29/Lys-6 preference. However, little sequence consensus was detected among conjugation sites, indicating that the local environment has little influence on global ubiquitylation. Intriguingly, the level of Lys-11–linked Ub polymers increased substantially upon MG132 treatment, revealing that they might be important signals for proteasomal breakdown. Taken together, this proteomic analysis illustrates the breadth of plant processes affected by ubiquitylation and provides a deep data set of individual targets from which to explore the roles of Ub in various physiological and developmental pathways.

INTRODUCTION

It is now abundantly clear that plant proteins are subjected to a wide array of posttranslational modifications that greatly expand proteome functionality from more limited genomic information. These modifications are often genetically predetermined, interconnected, and highly dynamic, thus providing near unlimited layers of control across a protein's life span. Among over 300 possibilities (Kwon et al., 2006), the 76–amino acid protein ubiquitin (Ub) has emerged as a dominant modifier based on its myriad likely targets and the breadth of processes under its influence (Smalle and Vierstra, 2004; Dreher and Callis, 2007; Vierstra, 2009; Santner and Estelle, 2010). Via an ATP-dependent conjugation cascade sequentially engaging E1, E2, and E3 Ub ligase enzymes, one or more Ub moieties become covalently attached through an isopeptide bond involving the C-terminal Gly of Ub. Typically, free lysl ε-amino groups in the targets serve as the acceptors, but instances where the Ub moiety is linked to the N-terminal amino group or to internal Ser, Thr, or Cys residues have been observed (Iwai and Tokunaga, 2009; Shimizu et al., 2010; Okumoto et al., 2011). A family of unique proteases collectively called deubiquitylating enzymes (DUBs) also participates, which reverses Ub addition by specifically cleaving Ub peptide/isopeptide linkages.

Ubiquitylation modifies proteins in a number of ways, which in turn confers additional structural information related to the fate of individual targets. These include monoubiquitylation, multi-ubiquitylation (the attachment of single Ubs to different Lys residues), and polyubiquitylation (the assembly of isopeptide-linked Ub chains in which any one of the seven Ub Lys residues might provide sites for polymerization) (Husnjak and Dikic, 2012; Komander and Rape, 2012). A unique situation found thus far only in mammals involves the assembly of peptide-linked linear Ub chains connected through the N-terminal Met (Iwai and Tokunaga, 2009). A prevalent fate is to commit proteins to degradation by the 26S proteasome using the addition of Lys-11– and Lys-48–linked poly-Ub chains as signals. This ~64-subunit, ATP-dependent proteolytic machine employs several Ub receptors that recognize the Ub polymers and then degrades the modified target concomitant with the DUB-directed release of the Ub moieties for reuse (Finley, 2009). Whereas some proteolytic targets undergo programmed ubiquitylation that selectively regulates their abundance, less target-specific ubiquitylation also occurs as part of a quality control system that removes misfolded and aggregated polypeptides (Ellgaard and Helenius, 2003; Shimizu et al., 2010). Large protein aggregates and unneeded multisubunit complexes are also cleared by autophagic processes following their ubiquitylation (Johansen and Lamark, 2011; Li and Vierstra, 2012). Alternatively, proteins subjected to monoubiquitylation or modified with Lys-63–linked Ub polymers direct nonproteolytic outcomes often related to chromatin organization, transcription, DNA repair, and protein trafficking (Mukhopadhyay and Riezman, 2007).

Both genetic and genomic studies have amply demonstrated that programmed ubiquitylation substantially impacts most, if

[1] Address correspondence to vierstra@wisc.edu.
The author responsible for distribution of materials integral to the findings presented in this article in accordance with the policy described in the Instructions for Authors (www.plantcell.org) is: Richard D. Vierstra (vierstra@wisc.edu).
[W] Online version contains Web-only data.
www.plantcell.org/cgi/doi/10.1105/tpc.112.108613

not all, aspects of plant biology. These include controls on hormone signaling, chromatin structure and transcription, photomorphogenesis, entrainment of circadian rhythms, self-incompatibility, and defense against biotic and abiotic challenges via the directed turnover of key intracellular regulators such as histone H2B, phytochrome A (phyA), auxin/indole-3-acetic acid proteins, ETHYLENE-INSENSITIVE-3 (EIN3), ABSCISIC ACID-INSENSITIVE-5 (ABI5), the DELLA gibberellin response factors, jasmonic acid/ZIM-containing proteins, LONG HYPOCOTYL-5, and CONSTANS (Dreher and Callis, 2007; Vierstra, 2009; Santner and Estelle, 2010). Much of these effects are regulated by the E3 ligases that help choose appropriate substrates for ubiquitylation. Remarkably, plant genomes are predicted to encode hundreds to well over a thousand different E3s, implying that equally large arrays of targets exist (Stone et al., 2005; Vierstra, 2009; Hua and Vierstra, 2011; Hua et al., 2011). This E3 diversity is comparable to that for protein kinases (Chevalier and Walker, 2005), indicating that ubiquitylation likely rivals protein phosphorylation as the dominant posttranslational modification in the plant kingdom.

Clearly, full appreciation of ubiquitylation will require deep and accurate catalogs of affected proteins. Unfortunately, developing these catalogs for plants has been challenged by the sheer number of targets and the facts that the conjugated forms are typically present at low steady state levels, are often condition specific and transient, and can contain an array of Ub architectures involving one or more Ub moieties. The presence of DUBs is also a major complication given that their high activities in crude plant extracts effectively release the Ub moieties during conjugate enrichment (Vierstra and Sullivan, 1988; Maor et al., 2007).

Despite these hurdles, several recent proteomic studies with *Arabidopsis thaliana* have provided a glimpse into the plant ubiquitylome (i.e., the collection of proteins modified by Ub). In an initial study, Maor et al. (2007) exploited the Ub-associated domain (UBA) and Ub-interacting motif (UIM) from the *Arabidopsis* DUB UBP14 and the proteasomal receptor RPN10, respectively, to single-step enrich for Ub conjugates from cell suspension cultures. Tandem mass spectrometry (MS) analysis of these preparations reported 294 possible targets. Using the di-Gly–modified Lys remnant (Ub footprint) that is generated following trypsinization of isopeptide-linked targets as the signature for Ub addition (Peng et al., 2003), potential attachment sites were mapped for 56 substrates, including five of the seven Ub Lys residues. Manzano et al. (2008) and Igawa et al. (2009) subsequently used the UBA domain from mammalian p62 and the monoclonal Ub antibody FK2, respectively, to single-step enrich for Ub conjugates from intact seedlings, which led to the MS detection of 200 and 169 putative Ub targets. Unfortunately, because each of these three purification strategies employed nondenaturing conditions, it remains unclear which proteins are actual Ub conjugates as opposed to those that bind to the affinity matrices nonspecifically or through their association with bona fide conjugates. Such modest stringency might explain, in principle, why these three proposed ubiquitylome catalogs share few candidates (3 to 14% overlap).

To overcome this complication, Saracco et al. (2009) more recently developed a transgenic *Arabidopsis* line expressing a novel Ub gene [*hexa(6His-UBQ)*] expressing a 6His-tagged variant that readily enters the Ub conjugation/deconjugation cycle. Its use enabled a more stringent two-step affinity approach involving the Ub-binding region from human HHR23A (UBA1-stress-inducible [STI]-UBA2; hereafter called USU; Figure 1A) to first enrich under native conditions based on the Ub moiety followed by nickel-chelate affinity chromatography to further enrich under denaturing conditions based on the 6His moiety. A total of 90 targets were identified with Ub attachment sites mapped onto 15. This more rigorous MS analysis detected Ub-Ub linkages involving six of the seven Ub Lys residues, together with evidence for mixed-linkage poly-Ub chains, indicating that linear isopeptide as well as branch Ub polymers might be assembled in planta (Saracco et al., 2009).

Unfortunately, based on proteomic analyses of yeast and mammalian cells where thousands of targets have been reported (Peng et al., 2003; Kirkpatrick et al., 2005; Mayor et al., 2005; Tagwerker et al., 2006; Xu et al., 2010; Danielsen et al., 2011; Emanuele et al., 2011; Kim et al., 2011; Wagner et al., 2011), it is likely that the current ill-defined *Arabidopsis* ubiquitylome represents only a small fraction of that synthesized in vivo. Here, we developed a more robust catalog of Ub targets by combining the *hexa(6His-UBQ)* line (Saracco et al., 2009) with high sensitivity MS and an improved two-step affinity methods for Ub conjugate purification. Particularly helpful was the adoption of the tandem repeated Ub-binding entities (TUBEs) strategy developed by Rodriquez and coworkers (Hjerpe et al., 2009; Lopitz-Otsoa et al., 2010) that dramatically improves the purification stringency and yield of Ub conjugates by using concatenated Ub-interacting domains as affinity matrices. The list of almost 950 targets identified here from young green seedlings contains key factors regulating a wide range of biological events, including cellular transport, signal transduction, transcription, translation, RNA biology, proteolysis, and metabolism. Moreover, we found that the ubiquitylation status of many increases after treating seedlings with the proteasomal inhibitor MG132, implying that a majority are 26S proteasome substrates. A large database of Ub-attachment sites was also generated, which underscored the preferential use of several of the seven Ub Lys residues in forming poly-Ub chains. Collectively, this proteomic study illustrates the breadth of *Arabidopsis* processes affected by ubiquitylation and provides a general use strategy to more effectively describe the ubiquitylome in other plant species.

RESULTS

TUBEs Affinity Purification of Ub Conjugates from *Arabidopsis*

A main barrier in defining plant ubiquitylomes by MS has been the lack of affinity methods that can effectively enrich for Ub conjugates under stringent conditions. While several native Ub-binding domains have showed promise (Maor et al., 2007; Saracco et al., 2009), their low avidity for Ub and Ub polymers dampened yield and precluded the use of harsh wash conditions to remove contaminants. More recently, affinity capture with antibodies against the di-Gly remnant of Ub linkages following trypsin cleavage has been exploited, but this strategy constrains

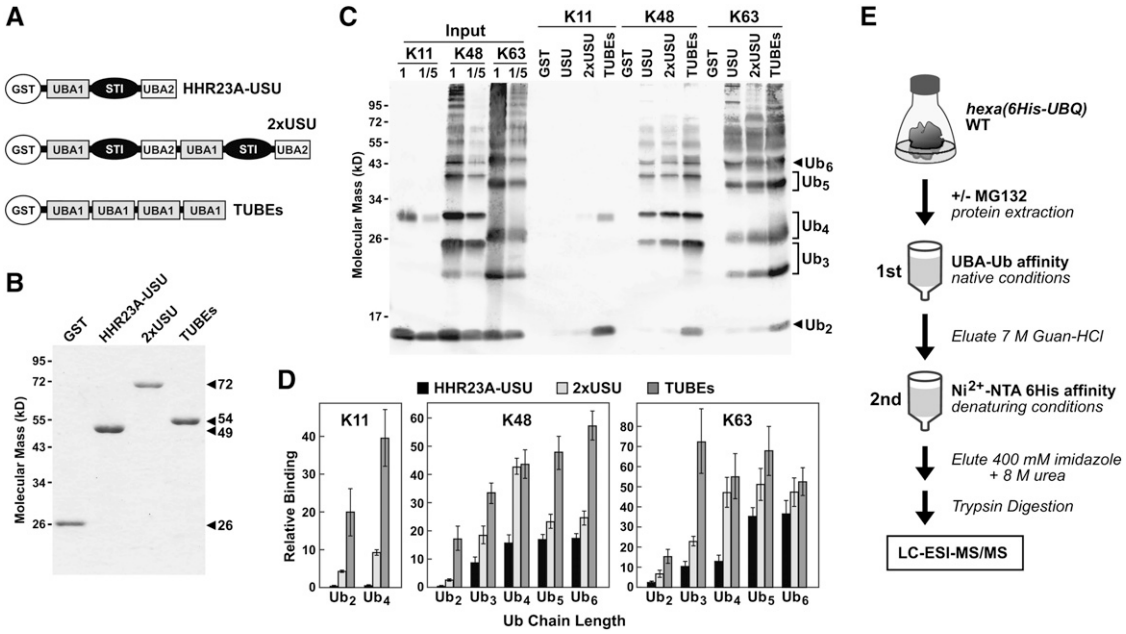

Figure 1. Use of Tandem Arrays of Ub-Binding Domains to Enrich for Ubiquitylated Proteins.

(A) Schematic representation of the GST-tagged versions of 2xUSU and TUBEs proteins generated from the USU region of human HHR23A.
(B) SDS-PAGE analysis of purified GST and the GST-tagged versions of USU, 2xUSU, and TUBEs. The calculated molecular masses are indicated.
(C) Poly-Ub chain binding in vitro. Mixtures of poly-Ub chains linked via either Lys-11 (K11), Lys-48 (K48), or Lys-63 (K63) were incubated with recombinant GST or GST fused to USU, 2xUSU, or TUBEs and precipitated with glutathione binding beads. The Ub moieties were resolved by SDS-PAGE and detected by immunoblot analysis with anti-Ub antibodies. The arrowheads and brackets to the right identify the various Ub polymers. Full strength (5 μg) and a fivefold dilution (1 μg) of each poly-Ub chain preparation are shown on the left.
(D) Quantification of poly-Ub chain binding efficiency for each Ub-binding domain by densitometric scanning of the immunoblots shown in **(C)**. Each bar represents the average (±SD) of three independent experiments.
(E) Flow chart describing the proteomic analysis of Ub conjugates isolated by two-step affinity protocols from intact *Arabidopsis* seedlings expressing 6His-Ub. The first purification step uses Ub affinity under native conditions followed by a second purification step that uses Ni-NTA affinity under denaturing conditions. ESI, electrospray ionization.

detection by providing only a single peptide with which to identify the parent protein and is further complicated by another Ub-fold protein Related-to-Ub-1 (or Nedd8) that generates an identical Lys-Gly-Gly isopeptide epitope when conjugated (Xu et al., 2010; Emanuele et al., 2011; Kim et al., 2011; Wagner et al., 2011). Hjerpe et al. (2009) recently improved affinity purification of intact conjugates by concatenating Ub-binding domains into artificial TUBEs. The prototype TUBEs not only showed strong cooperative avidity for Ub conjugates displaying various Ub linkages (K_d decreased 100- to 1000-fold relative to the monomeric domain), they effectively protected Ub conjugates upon binding from proteasomal degradation and disassembly by DUBs and other cellular proteases in vitro (Hjerpe et al., 2009; Lopitz-Otsoa et al., 2010).

Based on the TUBEs approach, we developed similar tandem matrices incorporating the Ub-binding UBA region from human HHR23A (Raasi et al., 2004). Either four individual UBA1 domains were concatenated head-to-tail by a short flexible linker (TUBEs) or the entire region in HHR23A encompassing the UBA1 and UBA2 domains separated by the STI domain was duplicated (2xUSU) in case the STI domain and/or the spacing between the UBA domains were critical to Ub polymer recognition (Figure 1A). These affinity matrices were fused to the C terminus of glutathione *S*-transferase (GST) to facilitate their isolation, and avoided the previously incorporated 6His tag so that they could be used in combination with a second nickel chelate-affinity step that exploits 6His-Ub (Saracco et al., 2009). As shown in Figure 1B, GST fusions of both the TUBEs and 2xUSU constructions, like their HHR23A USU parent, expressed well in *Escherichia coli* and could be easily purified with glutathione beads.

When tested for their ability to recognize Ub polymers of various linkage types, both the TUBEs and 2xUSU constructions proved superior compared with USU. Using a mixture of di- and tetra-Ub chains linked via Lys-11 or arrays of poly-Ub chains (two to more than seven Ub monomers) linked via Lys-48 or Lys-63 in GST pull-down assays, substantially more chains were recovered with TUBEs or 2xUSU (Figures 1C and 1D). TUBEs were particularly effective in binding Ub chains of all lengths. For example, whereas 2xUSU bound di- and tetra-Ub Lys-11–linked chains eightfold and 12-fold better than USU, respectively, TUBEs showed 49- and 68-fold better recoveries. Importantly, the TUBEs and 2xUSU matrices more effectively captured native Ub conjugates from *Arabidopsis* seedlings (see Supplemental Figure 1 online), with binding to the matrices maintained in NaCl concentrations up to 2 M and efficient elution requiring high concentrations of strong denaturants such as guanidine-HCl or urea.

By incorporating TUBEs and 2xUSU affinity chromatography, we then developed the two-step purification strategy outlined in Figure 1E that was optimized for both stringency and yield. Crude extracts from liquid-grown *hexa(6His-UBQ)* seedlings grown under continuous white light were prepared with a non-denaturing buffer containing Triton X-100 and amended with a cocktail of protease inhibitors to minimize DUB activities. Preliminary studies shown that this cocktail effectively protected both Ub conjugates and free 6His-Ub from disassembly by DUBs and/or degradation by other proteases (see Supplemental Figure 2 online). After clarification, the extracts were applied directly to the TUBEs or 2xUSU columns followed by washing with 2 M NaCl, and the bound conjugates were released with 7 M guanidine-HCl. The main contaminants after this step were ribulose-1,5-bis-phosphate carboxylase/oxygenase and either the GST-TUBEs or GST-2xUSU proteins or their breakdown products that bled from the beads. The denatured eluates were then applied to a nickel nitrilotriacetic acid (Ni-NTA) affinity column and sequentially washed with 6 M guanidine-HCl and 8 M urea before final release of ubiquitylated proteins with 8 M urea plus 400 mM imidazole. As shown in Figure 2, both TUBEs and 2xUSU effectively enriched for Ub conjugates but not free or dimeric Ub from *hexa(6His-UBQ)* plants as judged by staining for total protein and by immunoblot analyses with anti-Ub and anti-5His antibodies when compared with wild-type plants combined with GST and Ni-NTA columns. The greatest source of contaminants likely arose from the Ni-NTA step, some of which could represent proteins that bind nonspecifically to the Ni-NTA resin possibly through internal His-rich tracts. This contamination could be observed when comparing wild-type and *hexa(6His-UBQ)* seedling purified in parallel by the TUBEs and Ni-NTA affinity steps (see Supplemental Figure 3 online).

Liquid Chromatography–Tandem MS Identification of Ubiquitylated Proteins

The purified Ub conjugates were analyzed by tandem MS (MS/MS) using the Velos LTQ mass spectrometer, which provides both higher accuracy and faster sampling times compared with the spectrometers used previously with *Arabidopsis* (Maor et al., 2007; Manzano et al., 2008; Igawa et al., 2009; Saracco et al., 2009). Trypsinized peptides were separated by reversed-phase nanoflow liquid chromatography (LC) followed by MS/MS sequencing in the high energy collision (HCD) mode, and the peptide spectra were searched against the *Arabidopsis* ecotype Columbia-0 (Col-0) proteome database (IPI database version 3.85; http://www.Arabidopsis.org) using SEQUEST. A likely Ub conjugate was included in the ubiquitylome catalog based on the MS identification of two or more different matching peptides with a $\leq$1% false discovery rate (FDR) or if a single matching peptide of equivalent stringency was identified with a canonical Ub footprint. These footprints were detected as a missed Lys trypsin cleavage together with an increased mass of 114 D for the modified Lys as a result of the appended di-Gly remnant (Lys-Gly-Gly; Peng et al., 2003). Importantly, because iodoacetamide can confuse MS/MS detection of such Ub footprints by forming adducts with Lys residues of equivalent mass (Nielsen et al., 2008), we used chloroacetamide instead to inhibit Cys proteases in the crude extracts and to subsequently carboxymethylate Cys residues before MS analysis of the tryptic peptides.

To help eliminate protein contaminants that bind nonspecifically to the matrices, we also generated a background MS data set obtained by mock purification of wild-type seedlings with sequential GST and Ni-NTA columns, which was subtracted from all final ubiquitylome data sets (see Supplemental

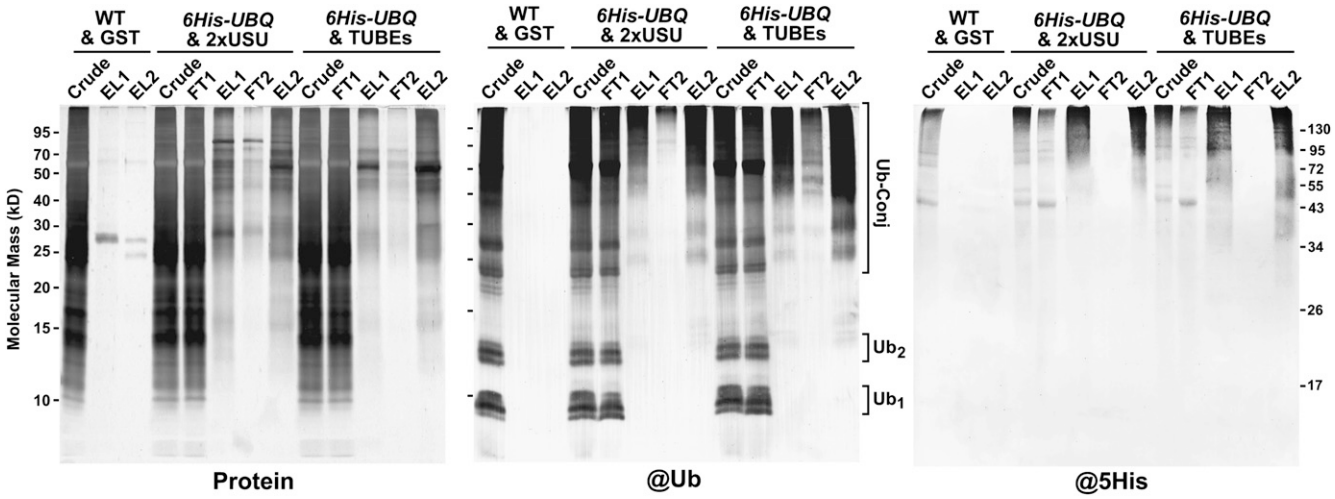

Figure 2. Two-Step Affinity Purification of Ubiquitylated Proteins from Transgenic *Arabidopsis* Expressing 6His-Ub.

Ub conjugates were purified from *hexa(6His-UBQ)* seedlings by the two-step protocol outlined in Figure 1E and subjected to SDS-PAGE. The gels were either stained for total protein with silver or immunoblotted with anti-Ub or anti-5His antibodies. Samples from wild-type seedlings (WT) subjected to the same purification with GST and Ni-NTA beads were included for comparison. FT and EL represent the flow-through and elution, respectively, from the Ub affinity (1) and Ni-NTA affinity columns (2). "Crude" represents the clarified crude extracts before purification. The migration position of free Ub, the Ub dimer, and Ub conjugates are indicated on the right of the anti-Ub antibody blot.

Data Set 1 online). A total of 240 contaminants were identified based on the detection of two or more different peptides from at least one of eight biological replicates. Fifteen were found in all eight analyses and thus represent common false positives, while 87 (37%) were detected only once in eight tries and may represent stochastic detection and not contaminants. We acknowledged that some of these false positives might be ubiquitylation targets. In fact, four such contaminants (GAPC1, GAPC2, ADH1, and EMB1080) were removed from this list based on our subsequent detection of obvious Ub footprints within daughter tryptic peptides.

We first analyzed the ubiquitylome from young *hexa(6His-UBQ)* seedlings using either TUBEs and 2xUSU chromatography combined with Ni-NTA chromatography, which lead to the detection of 340 and 379 putative ubiquitylated targets, respectively (Figures 3A and 3B). The TUBEs and 2xUSU MS data sets each had an ~61% overlap among three biological replicates, suggesting that the catalogs of targets detected were not yet saturated (see Supplemental Figure 4A online). Surprisingly, only a 53% overlap among targets was observed (248 of 471) when comparing the combined lists from the TUBEs and 2xUSU matrices, strongly suggesting that they captured partially distinct fractions of the ubiquitylome presumably via different affinities for various Ub chain architectures. Notable examples enriched only by 2xUSU include CDC6 and two ferritin and copper/zinc superoxide dismutase paralogs, whereas those specifically enriched by TUBEs include members of the adaptin and α/β-hydrolases superfamilies and mitogen-activated protein (MAP) kinases (see Supplemental Data Set 2 online).

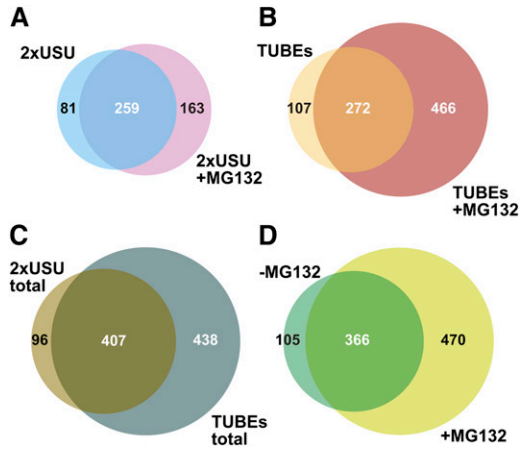

Figure 3. Venn Diagrams Showing the Overlap of Ubiquitylated *Arabidopsis* Proteins Identified by MS from Samples Purified using 2xUSU or TUBEs.

(A) and **(B)** Overlap of ubiquitylated proteins isolated using 2xUSU or TUBEs with or without pretreatment of the *Arabidopsis* seedlings with MG132.

(C) Overlap of ubiquitylated proteins isolated using 2xUSU and TUBEs.

(D) Overlap of the complete list of ubiquitylated proteins purified via the 2xUSU and TUBEs matrices from seedlings with or without pretreatment with MG132.

Because ubiquitylation often commits proteins to proteasomal turnover, we also analyzed in triplicate liquid-grown seedlings treated for 12 h with 50 μM of the proteasomal inhibitor MG132 to increase the stability and, thus, abundance of this fraction. Preliminary studies showed that this exposure was sufficient to attenuate autocatalytic processing of the proteasome β1 subunit PBA1 in planta, which is known to be MG132 sensitive (Book et al., 2010), and to detectably increase the pool of Ub conjugates (see Supplemental Figure 5 online). MS analysis of MG132-treated seedlings led to the detection of 422 and 738 Ub conjugates following 2xUSU and TUBEs enrichment, respectively, with substantial overlap among triplicates (Figures 3A and 3B; see Supplemental Figure 4A online). After subtracting contaminants and eliminating duplicates, a cumulative list of 941 putative ubiquitylation substrates was generated (see Supplemental Data Set 2 online), a majority (90%) of which was captured with the TUBEs matrix (Figure 3C) in line with its stronger affinity for poly-Ub chains. Collectively, 105 substrates were detected only in the absence of MG132, 366 were detected in both control and MG132-treated seedlings, and 470 were evident only in MG132-treated seedlings, implying that many ubiquitylated targets are substrates of the 26S proteasome (Figure 3D).

As expected, the dominant peptides in our MS data sets were derived from Ub, which represented ~15% of total peptide spectral matches (PSMs). The 50 next most abundant targets based on PSMs were generally involved in metabolism, cellular transport, protein fate, and protein synthesis (see Supplemental Data Set 3 online) in line with prior MS studies of the *Arabidopsis* ubiquitylome (Maor et al., 2007; Saracco et al., 2009). We note that 791 of the 941 ubiquitylated proteins detected here (84%) were not found by previous studies. The best overlap (37%) was with the partial ubiquitylome catalog generated by Saracco et al. (2009) that also incorporated the USU region from HHR23A and Ni-NTA resins in a two-step purification strategy (33 of its 90 targets in common).

Gene Ontogeny Analyses of Ubiquitylated Targets

As a first step toward understanding the global ramifications of ubiquitylation, we binned the 941 targets based on their known or predicted functions using the gene ontogeny (GO) classifications in MIPS-FunCat (Ruepp et al., 2004). To avoid duplicate classifications and thus simplify the analysis, we manually rebinned the GO listing of the full *Arabidopsis* proteome such that each protein was assigned solely to its best predicted classification in MIPS. Compared with the GO analysis of the 27,430 proteins annotated to date in the complete *Arabidopsis* proteome, the ubiquitylome catalog was enriched for proteins involved in metabolism (24% versus 12%), cellular transport (12% versus 8%), protein synthesis (10% versus 2%), and energy (7% versus 2%) but underrepresented for proteins involved in transcription (3% versus 7%) or not yet classified (11% versus 35%) (Figures 4A and 4C). We then further subdivided the 941 members of the ubiquitylome into those proteins whose MS detection was either increased or unaffected/decreased by proteasomal inhibition with MG132. The unaffected/reduced targets included those detected only in untreated seedlings (105) or in

both MG132-treated and untreated seedlings but with PSM differences less than threefold (266). The increased targets included those proteins only detected in MG132-treated seedlings (470) or detected in both mock and treated seedlings but had greater than or equal to threefold more PSMs upon MG132 exposure (100 of 366 targets). On average, PSMs for the 100 proteins that met the threefold cutoff increased by 4.8-fold upon MG132 treatment compared with 1.3-fold for contaminants and 1.3-fold for the 266 Ub targets unaffected or reduced in abundance by MG132. It was possible that the greater than or equal to threefold increase in PSMs upon MG132 treatment was strongly influence by low PSM numbers given the sometimes stochastic nature that low abundance proteins are detected by MS/MS. However, this does not appear to have a strong affect here. In a plot of PSM counts (2 to >30 PSMs) relative to the PSM ratio ±MG132, a slope of only 0.062 was obtained for the 366 ubiquitylated proteins that were detected in both control and MG132-treated data sets (see Supplemental Figure 6 online).

Presumably, the MG132-increased collection (570) would be enriched for 26S proteasome substrates, whereas the unaffected/reduced collection (371) would be enriched for proteins in which ubiquitylation directs autophagic turnover or other nonproteolytic outcomes. Regardless, the two subgroups had similar GO distributions with a slight enrichment for proteins dedicated to metabolism and signal transduction in the MG132-increased group (Figures 4D and 4E).

It was possible that at least part of the GO classification differences between the entire *Arabidopsis* proteome and the ubiquitylome reflected intrinsic variations in protein abundance among the GO categories, which would unavoidably impact MS discovery of the entire ubiquitylome. As examples, it is likely that many metabolic enzymes are more abundant compared with transcriptional regulators, which in turn might favor their MS detection generally even if their depth of ubiquitylation was comparable. Conversely, the underrepresentation of the unclassified bin could reflect the possibility that many of these proteins are in fact poorly expressed or are the predicted but not realized products of pseudogenes and thus would evade MS detection regardless of ubiquitylation state. To test for such biases, we also generated a MS data set of abundant *Arabidopsis* proteins amenable to detection (MS-detectable) by direct LC-MS/MS analysis in triplicate of trypsinized crude seedling extracts without prior fractionation. In total, 1013 proteins were identified with two or more matching peptides, 404 of which were detected in all three biological replicates and 644 in at least two MS runs (see Supplemental Figure 4B online). As expected, the most abundant proteins based on PSMs were the large and small subunits of ribulose-1,5-bis-phosphate carboxylase/oxygenase and other chloroplast proteins (see Supplemental Data Set 4 online).

Like the ubiquitylome, this MS-detectable proteome was noticeably enriched in factors related to metabolism, energy, protein synthesis, and cell rescue and defense but depleted in those involved in transcription (Figure 4B). However, while the percentages of the MS-detectable proteome in each GO category had a similar distribution as the ubiquitylome (e.g., overrepresentation of metabolism and underrepresentation of transcription), there was little overlap in the two lists (29%). This poor overlap was best seen by subdividing the MS-detectable proteome and the ubiquitylome into the different GO categories (Figure 4F). As an example, for the 1875 predicted transcription factors, we detected nine in the crude extracts, only one of which overlapped with the 31 identified ubiquitylation targets. Conversely, we found 159 of the 3252 metabolic proteins in the crude extracts, only 80 of which overlapped with the 225 targets of ubiquitylation. As might have been expected, the MS-detectable proteome had the best overlap with the list of contaminants (69%), implying that many contaminants are high-abundance proteins amenable to MS detection that bind nonspecifically to the affinity columns. Taken together, while our ubiquitylome database does contain a slight bias for abundant proteins and/or those more easily detected by tandem MS, the majority are less abundant and with a different collective GO enrichment relative to the entire *Arabidopsis* proteome.

Protein Interaction Networks for the *Arabidopsis* Ubiquitylome

To help appreciate how ubiquitylation might impact *Arabidopsis* physiology and development, we generated an interaction network using the Search Tool for the Retrieval of Interacting Genes/Proteins database (Szklarczyk et al. 2011) that detected associations among 440 proteins with a high confidence score (0.70). As shown in Figure 5, this network identified a complex interconnected web with a number of ubiquitylated proteins present at key hubs. Especially enriched were subnetworks involved in general and sugar metabolism, ribosome assembly/translation, 26S proteasome composition, membrane transport (aquaporins and H^+-ATPases), protein folding and transport, and RNA biology. Within the 26S proteasome, 19 of the 26 core subunits were found to be ubiquitylated, including a majority of the isoform pairs. Similar to studies with other eukaryotes (Xu et al., 2010; Danielsen et al., 2011; Emanuele et al., 2011; Kim et al., 2011; Wagner et al., 2011), our *Arabidopsis* ubiquitylome catalog was also notably enriched in other UPS components (i.e., E2, E3s, DUBs, and accessory proteins; see Supplemental Data Set 2 online), suggesting that such autoubiquitylation has regulatory consequences or might simply reflect collateral damage caused by their proximity to the Ub-transfer machinery.

A number of enzymes connected to various aspects of metabolism were prominent in the ubiquitylome network, ranging from carbohydrate metabolism and glycolysis/gluconeogenesis to secondary metabolism and nitrate assimilation (Table 1, Figure 5; see Supplemental Data Set 2 online). Within the phenylpropanoid biosynthetic pathway alone, many crucial enzymes were detected, including PAL, C4H, HCT, CAD, and OMT1, which convert Phe to anthocyanin, 4-coumaroyl alcohol, and/or lignin precursors, indicating that its throughput might be substantially regulated by ubiquitylation (see Supplemental Figure 7 online). Notable examples in carbohydrate metabolism include several paralogs of phosphoenolpyruvate (PEP) carboxylase and Suc synthase, the cytoplasmic isoforms of phosphofructokinase, and trehalose phosphatase, phosphoglucomutase, aldolase, and several UDP glucosyltransferases that occupy key cytosolic steps in sugar formation and metabolism. Previous studies showed that PEP carboxylase in the endosperm of germinating castor bean (*Ricinus communis*) seeds is monoubiquitylated at

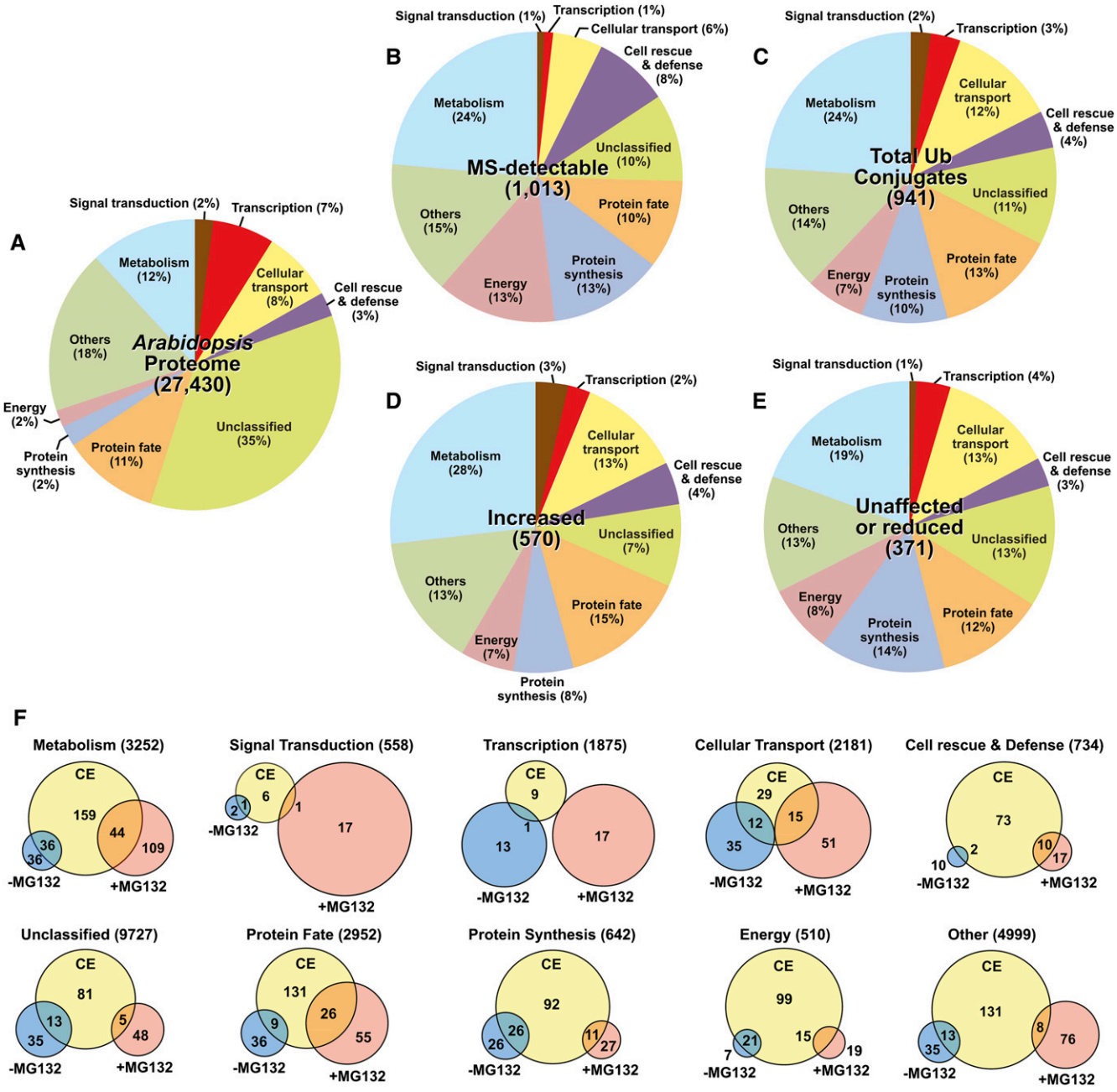

Figure 4. Sorting of Ubiquitylated *Arabidopsis* Proteins into Functional Categories.

The percentages of proteins in each data set were classified into functional categories using the GO annotations in the MIPS-FunCat database.
(A) The complete *Arabidopsis* proteome of 27,430 proteins.
(B) The 1013 proteins identified by MS analysis of crude extracts from green wild-type seedlings prior to enrichment.
(C) The combined list of 941 ubiquitylated proteins isolated from *hexa(6His-UBQ)* seedlings using either 2xUSU or TUBEs followed by Ni-NTA affinity chromatography.
(D) Those proteins in **(C)** that became more abundant or were solely detected after MG132 treatment of seedlings.
(E) Those proteins in **(C)** whose levels were unaffected or reduced after MG132 treatment of seedlings.
(F) Overlap of *Arabidopsis* proteins from each functional category based on their MS detection in crude seedling extracts (CE) and in the MS data sets of affinity-purified ubiquitylated proteins obtained from seedling exposed to DMSO (−MG132) or MG132 (+MG132). The numbers associated with each space represents the total number of MS-detected proteins for that space. The number at the top of each Venn diagram represents the total number of proteins in each category for the complete *Arabidopsis* proteome.

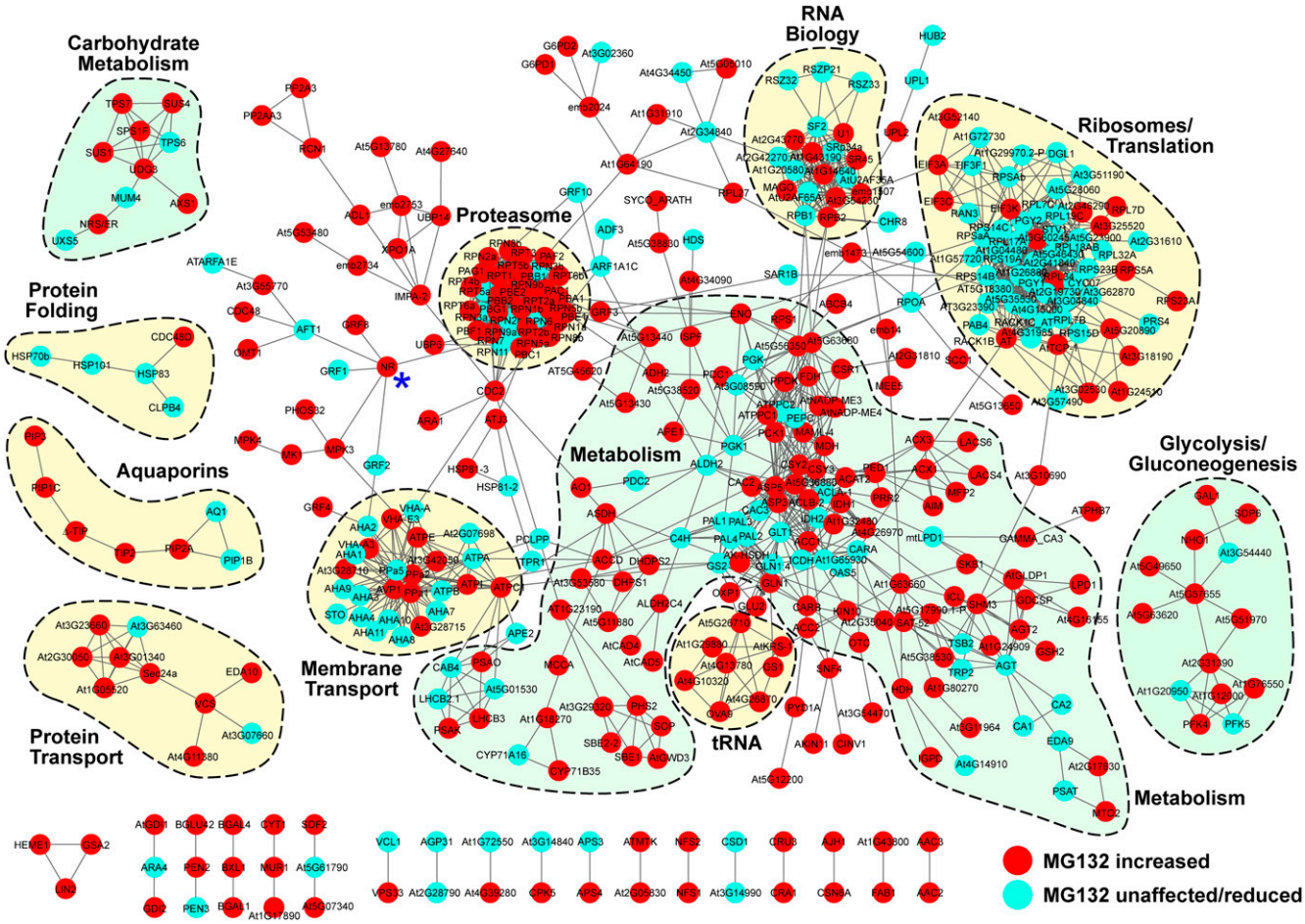

Figure 5. Protein Interaction Networks of Identified Ubiquitylated Proteins.

Protein interaction networks were generated with the complete list of ubiquitylated proteins using the Search Tool for the Retrieval of Interacting Genes/Proteins database and visualized using the Cytoscape program. The networks shown were restricted to those with at least one interaction. The node colors reflect ubiquitylation states that increased (red) or were unaffected or reduced (stable/reduced; blue) upon MG132 treatment based on PSMs. Important functional clusters are surrounded by dashed lines. Blue asterisk locates nitrate reductase. Either the *Arabidopsis* locus identifier or the protein name abbreviation (where known) is shown for each substrate.

Lys-628, a strictly conserved residue within the family, and that this modification has a regulatory as opposed to a proteolytic function by controlling substrate binding (Uhrig et al., 2008). In agreement, we detected three of the four PEP carboxylase isoforms in our *Arabidopsis* ubiquitylome catalog, which were either found only in −MG132 samples or were strongly reduced in abundance (approximately threefold) in samples treated with MG132.

A number of plastid-localized metabolic enzymes were present in the ubiquitylome. Their appearance could reflect contamination, or more interestingly, the UPS-mediated elimination of unimported or misfolded precursors as part of a quality control pathway (Shen et al., 2007; Lee et al., 2009), and/or the removal of integrated functional proteins as has recently been shown for subunits of the plastid TOC protein translocation complex following their ubiquitylation by an outer envelope-bound E3 (Ling et al., 2012). However, our hand analysis of four plastid-localized proteins that were abundant in our ubiquitylation data set failed to find peptides within the predicted N-terminal transit sequences, suggesting that these plastid proteins were ubiquitylated after processing. Nine of the 12 H^+-ATPases isoforms (AHA1-4 and 7-11), six aquaporin isoforms, and multiple components of the protein SEC secretory pathways were also prominent in the ubiquitylome list, implying an unanticipated control on proton, water, and protein transport by ubiquitylation. The modifications of these transporters could reflect a role for Ub in endocytosis and subsequent vacuolar breakdown of these and other integral membrane proteins in plants (Mukhopadhyay and Riezman, 2007; MacGurn et al., 2012).

Particularly notable, we found a web of ubiquitylated proteins connected to RNA silencing, abscisic acid, auxin, and brassinosteroid (BR) hormone signaling, circadian rhythms, nitrate metabolism, and innate immunity, suggesting that these processes are heavily influenced by Ub addition (Table 1). The ubiquitylation

Table 1. Examples of Pathways with Ubiquitylation Targets[a]

Name	Gene Locus	Function/Activity	MG132[b]
RNA Silencing			
AGO1	At2g48410	RNA splicer	+
AGO2[c]	At1g31280	RNA splicer	+
AGO10/PNH	At5g43810	RNA splicer	−
HEN2	At2g06990	RNA helicase	+
SE	At2g27100	RNA splicing	+
VCS	At3g13300	mRNA decapping	+
ABA Signaling			
PYR1	At4g17870	Abscisic acid receptor	+
SnRK1.1	At3g01090	Protein kinase	+
SnRK2.4	At1g10940	Protein kinase	+
OST1	At4g33950	Protein kinase	+
SUA	At3g54230	splicing factor	+
MPK3	At3g45640	MAP kinase	+
MPK4	At4g01370	MAP kinase	+
CDPK2 (CPK11)	At1g35670	Protein kinase	+
CDPK6 (CPK3)	At4g23650	Protein kinase	+
RCN1	At1g25490	Protein phosphatase	+
Auxin Signaling			
ABF4[c]	At4g24390	FBX auxin receptor	−
BIG/TIR3	At3g02260	Auxin transport	+
ABCB4	At2g47000	Auxin efflux	+
CAND1	At2g02560	CRL regulator	+
CSN5A	At1g22920	CSN CRL regulator	+
CSN6A	At5g56280	CSN CRL regulator	+
IBR5	At2g04550	Protein phosphatase	−
PP2A	At1g69960	Protein phosphatase	+
RCN1	At1g25490	Protein phosphatase	+
PP2A-A2	At3g25800	Protein phosphatase	+
PP2A-A3	At1g13320	Protein phosphatase	+
BR Signaling			+
ST1	At2g03760	BR sulfotransferase	+
ST4A	At2g14920	BR sulfotransferase	+
BSK1	At4g35230	Protein kinase	+
RCN1	At1g25490	Protein phosphatase	+
PP2A-A2	At3g25800	Protein kinase	+
PP2A-A3	At1g13320	Protein kinase	+
GRF10	At1g22300	14-3-3 Protein	−
Circadian Rhythms			
PRR7[c]	At5g02810	Pseudoresponse regulator	+
CKA1	At5g67380	Casein kinase	+
CKA2	At3g50000	Casein kinase	+
EPR1	At1g18330	Early Phy response transcription factor	−
Nitrate Metabolism			
NR2	At1g37130	Nitrate reductase	+
MPK3	At3g45640	MAP kinase	+
CDPK6 (CPK3)	At4g23650	Protein kinase	+
GRF1	At4g09000	14-3-3 Protein	−
GRF2	At1g78300	14-3-3 Protein	−
GRF3	At5g38480	14-3-3 Protein	+
GRF6	At5g10450	14-3-3 Protein	−
GRF8	At5g65430	14-3-3 Protein	+
Phenylpropanoid Metabolism			
PAL1	At2g37040	Phe ammonia lyase	−
PAL2	At3g53260	Phe ammonia lyase	−
PAL3	At5g04230	Phe ammonia lyase	−
C4H	At2g30490	Cinnamate-4-hydroxylase	−
HCT	At5g48930	HC-CoA transferase	+

(Continued)

Table 1. (continued).

Name	Gene Locus	Function/Activity	MG132[b]
CAD	At1g72680	Cinnamyl alcohol dehydrogenase	−
COMT	At5g54160	Caffeic methyltransfer	+
Innate Immunity			
PCS1	At5g44070	Phytochelatin synthase	−
PEN2	At2g44490	β-Glucosidase	+
PEN3	At1g59870	ABC transporter	−
PAD2	At4g23100	Glu-Cys ligase	+

[a]See Supplemental Data Set 2 online for the complete list.
[b]Plus and minus signs identify ubiquitylated proteins whose PSM abundance either increased (+) or remained the same or decreased (−) upon treating the plants with MG132.
[c]One or more Ub-binding sites mapped (see Supplemental Data Set 5 online).

status of most of these targets increased upon MG132 treatment, implying subsequent engagement by the 26S proteasome. The impacted components for RNA silencing include several members of the ARGONAUTE (AGO) family, the SE component of the RNA-induced silencing complex, and the HEN2 RNA helicase and VCS mRNA decapping factors. Ubiquitylation of AGO1 in particular might be related to its turnover by autophagy (Gibbings et al., 2012; Derrien et al., 2012). Ubiquitylated components in BR signaling include the ST1 and ST4A BR sulfotransferases required for BR synthesis, the immediate substrate of the BRI1 receptor kinase (BSK1), and several PP2A protein phosphatases and the 14-3-3/General Regulatory Factor (GRF) protein GRF10 that direct downstream steps (Table 1).

The detection of multiple proteins in our ubiquitylation data sets that are known or might exist in complexes (e.g., 26S proteasome and ribosome subunits) raised that possibility that some of our proposed targets are not ubiquitylated but were enriched by their association with other ubiquitylated proteins even under the harsh purification conditions used (8 M urea and 7 M guanidine-HCl). To discount this possibility, we examined the stability of the 26S proteasome under such denaturing conditions. Here, crude extracts were prepared under native conditions from *Arabidopsis* seedlings in which the PAG1 (α7) subunit was replaced with a Flag-tagged version (Book et al., 2010). The extracts were made 8 M urea or 7 M guanidine-HCl in an attempt to denature the complex, and the denaturants were subsequently diluted or removed by dialysis. We then attempted to enrich for the entire 26S proteasome by anti-Flag affinity chromatography. As shown in Supplemental Figure 8 online, both denaturants substantially dissociated PAG1 from the rest of the 26S proteasome, even in the presence of ATP, which stabilizes the association of the regulatory particle with the core protease (Book et al., 2010). Whereas the PAG1-Flag protein and other subunits of the core protease complex (±ATP) and/or regulatory particle (+ATP) were efficiently isolated together under native conditions, only PAG1-Flag was isolated with the anti-Flag beads following treatment with the denaturants.

Contrasting Effects of Ubiquitylation on the Proteasome and Ribosome

When the interactome network of Ub conjugates was assessed globally for concerted effects of MG132, a surprising contrast was observed for 26S proteasome versus the translation machinery. While the abundance of most, if not all, ubiquitylated 26S proteasome subunits increased significantly upon proteasomal inhibition (average of 3.9-fold), most ubiquitylated components of the ribosome were unaffected/reduced (Figures 5 and 6; see Supplemental Data Set 2 online). PSMs for 28 of the 36 proteasome core subunits (78%) were increased threefold to 11-fold by MG132 and the remaining eight increased (RPT2b, RPT4b, RPT5a, RPN2b, RPN3a, RPN3b, RPN9a, and RPN11) by a collective average of 2.0-fold. The ubiquitylation of the core protease capping proteins PA200 and CDC48 was similarly increased (PA200 was identified in the MS data sets only after MG132 treatment, and CDC48 displayed a ninefold increase with +MG132). The unmodified pools of representative proteasome proteins, PA200 and CDC48, also rose upon MG132 exposure, suggesting that this increased ubiquitylation is connected to turnover of inhibited proteasome complexes (Figure 6B).

In agreement with previous studies using *Arabidopsis* (Maor et al., 2007; Saracco et al., 2009) and other eukaryotes (Peng et al., 2003; Xu et al., 2010; Emanuele et al., 2011; Kim et al., 2011; Wagner et al., 2011), we found that many subunits of both the 40S and 60S ribosome complexes are ubiquitylated (56 in total). But in contrast with the proteasome, the average fold increase in PSMs −/+MG132 for all ribosomal subunits detected was only 1.2-fold with the ubiquitylation status on most (77%) unchanged or reduced by the inhibitor (Figures 5 and 6A). As examples, the ubiquitylation state of the 40S subunits RPS3 and RPS5 dropped by 1.7- and 1.1-fold after MG132 exposure, respectively. Immunoblot analysis of RPS3 and RPS5 also revealed that MG132 significantly reduced in parallel the pool of the unmodified forms (Figure 6B), suggesting that this drop in ubiquitylation is linked to a drop in ribosome number potentially by increasing turnover via a non-UPS mechanism (see below).

Mapping Attachment Sites on Individual Ub Conjugates

Using the canonical Lys-Gly-Gly isopeptide footprint as a signature for Ub attachment, we greatly increased the number of known Ub-binding sites. In total, 120 ubiquitylation sites were mapped onto 109 proteins (see Supplemental Data Set 5 online). All sites were newly mapped except for those identified previously within casein lytic proteinase B3, CDC48, glyceraldehyde-3-phosphate dehydrogenase, heat shock protein 81-3, and the

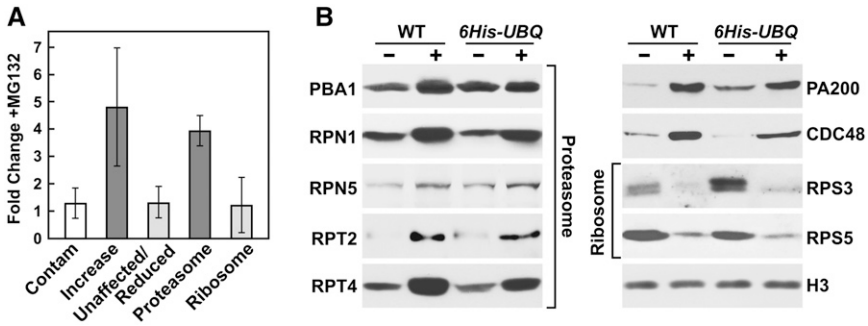

Figure 6. The Abundance of Proteasome- and Ribosome-Associated Proteins Are Inversely Affected by MG132.

(A) Fold change in ubiquitylated protein abundance based on MS PSMs after a 12-h pretreatment of seedlings with 50 μM MG132. Each bar represents the average of three independent experiments (±SD). Ubiquitylated proteins were purified by the 2xUSU or TUBEs matrices from *hexa(6His-UBQ)* seedlings. Increased category includes 100 ubiquitylated proteins with a greater than or equal to threefold increase in PSMs. Unaffected/reduced category includes 266 ubiquitylated proteins with less than threefold change in PSMs. Proteasome and ribosome categories include 20 and 36 ubiquitylated proteins, respectively. Contam category represents 50 proteins that were purified from wild-type seedlings by sequentially GST and Ni-NTA chromatographic steps.

(B) Levels of proteasome-associated proteins increase, whereas ribosome proteins decrease in abundance upon MG132 treatment. Crude extract proteins from 10-d-old seedlings [the wild type (WT) and *hexa(6His-UBQ)*] with or without MG132 treatment were separated by SDS-PAGE and subjected to immunoblot analysis with antibodies that recognize the proteasome subunits PBA1, RPN1, RPN5, RPT2, and RPT4, the proteasome accessory factors PA200 and CDC48, and the ribosome 40S particle subunits S3 (RPS3) and S5 (RPS5). Anti-histone H3 antibodies were used to confirm equal protein loading.

Leu-rich repeat family protein At3g20820 (Maor et al., 2007; Saracco et al., 2009). Two footprints were detected on 13 proteins, indicating that multiubiquitylation or polyubiquitylation at different sites occurs in *Arabidopsis*. We also searched the MS/MS spectra for Gly-Gly remnants reflecting noncanonical linkages previously found in other eukaryotes involving the N-terminal residue, Ser, Thr, or Cys (Iwai and Tokunaga, 2009; Shimizu et al., 2010; Okumoto et al., 2011). None were detected, suggesting that such alternatives are either not used by plants or are at levels that evaded our detection.

One hope from such a comprehensive list of Ub attachment sites was that a consensus motif(s) directing Ub addition would emerge. However, our combined analysis of the Ub-binding site lists developed here and elsewhere (Maor et al., 2007; Saracco et al., 2009; Book et al., 2010) suggests that such universal motif (s) do not exist. Alignment by IceLogo (Colaert et al., 2009) of the sequence window six residues N- and C-terminal to the modified Lys for 216 mapped Ub-binding sites derived from 182 proteins failed to detect a strong consensus ubiquitylation motif (see Supplemental Figure 9 and Supplemental Data Set 5 online). However, like previous studies with the human ubiquitylome (Kim et al., 2011), there was a subtle enrichment for acidic residues surrounding the linkage site along with a general avoidance of bulky hydrophobic residues. Whether these weak biases reflect specific ubiquitylation sequences used by subclasses of targets or the more general requirement that the modified Lys be in a solvent-exposed, hydrophilic region is not yet known.

Analysis of Poly-Ub Linkages

As in previous MS studies (Maor et al., 2007; Saracco et al., 2009), searches of our data sets also found numerous PSMs for Ub peptides bearing Lys-Gly-Gly footprints reflecting isopeptide linkages within poly-Ub chains. In total, 1009 Ub footprint PSMs were recorded from 12 replicate MS experiments that mapped to six of the seven Ub Lys residues (Figure 7A). Lys-27 was the only Lys not identified as participating in poly-Ub chain assembly, consistent with the fact that its ε-amino side chain appears to be protected from the solvent in the three-dimensional structure of Ub (Figure 7A). Despite having a larger data set of Ub footprint peptides compared with our previous study (Saracco et al., 2009), we failed to detect Ub peptides bearing footprints on both Lys-29 and Lys-33, thus raising doubts as to the proposed assembly of branched chains with these residues. Based on the percentages of each footprint in the total PSM counts of Ub footprint peptides, a chain linkage preference of Lys-48>Lys-63>Lys-11>>>Lys-33/Lys-29/Lys-6 was found, which is consistent with previous proteomic studies in other eukaryotes and that by Maor et al. (2007) with *Arabidopsis*. The same rank order was generated from samples prepared with either the TUBEs or 2xUSU affinity columns, in line with the similar affinity of these two ligands for various types of poly-Ub chains (Figures 1C and 1D). However, this preference was notably distinct from the prior study of Saracco et al. (2009), which rarely found Lys-63 linkages in preparations affinity enriched with just a single USU region, suggesting that recovery of Lys-63–linked chains is substantially enhanced by the TUBEs strategy. Also in agreement with in vitro binding data (Figure 1D), Lys-11 linkages were more commonly detected in the TUBEs and 2xUSU preparations than previously reported by us (Figures 7B and 7C). We failed to find Gly-Gly footprints attached to the N-terminal Met of Ub, suggesting either that the matrices used here bind such conjugates poorly or that linear chains are not assembled in planta.

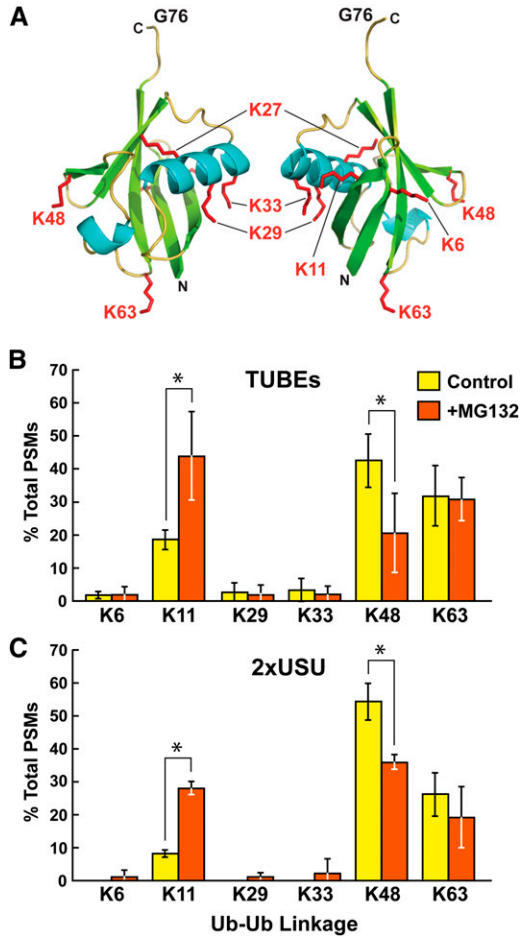

Figure 7. The Distribution of Intra-Ub–Ub Linkages and Their Changes in Abundance upon Treating *Arabidopsis* with MG132.

(A) Three-dimensional ribbon front and side diagrams of plant Ub highlighting the Lys residues that could bind Ub covalently. α-Helices, β-strands, and the side chains of Lys residues are shown in cyan, green, and red, respectively. N, N terminus; C, C terminus; G76, C-terminal active-site Gly. Adapted from Protein Data Bank code 1UBQ (Vijay-Kumar et al., 1987).

(B) and (C) Percentage of Ub footprints identified by MS/MS that represent Ub chains linked internally through the various Ub Lys residues. Ubiquitylated proteins were purified with TUBEs (B) or 2xUSU (C) from seedlings with or without pretreatment with 50 μM MG132. Each bar represents the average of three independent MS analyses (±SD). Asterisks indicated significant differences as determined by the Student's *t* test ($P < 0.05$).

Surprisingly, when seedlings exposed to MG132 were examined for Ub chain preferences, we found a significant shift from Lys-48– to Lys-11–linked chains. Whereas the relative percentages of Lys-6–, Lys-29–, Lys-33–, and Lys-63–linked chains were not significantly altered by pretreating the seedling for 12 h with 50 μM MG132, the percentages of Lys-11–linked chains rose substantially (2.4- to 3.5-fold) along with a reciprocal drop in the percentages of Lys-48-–linked chains (2.1- to 1.5-fold) in samples affinity purified by either the TUBEs or 2xUSU matrices, respectively (Figures 7B and 7C). Lys-48–linked chains, especially those containing four or more Ub monomers, are the principal signals in 26S proteasome–mediated turnover of ubiquitylated proteins (Finley, 2009; Kim et al., 2011; Wagner et al., 2011), whereas Lys-11 had been implicated in more selective breakdown associated with endoplasmic reticulum-associated degradation (ERAD) and the cell cycle (Jin et al., 2008; Xu et al., 2009). Consequently, this shift in poly-Ub chain abundance by MG132 could reflect a selective stabilization of specific classes of targets (e.g., ERAD) either directly or indirectly as a consequence of proteotoxic stress induced by proteasomal inhibition (Kim et al., 2011).

DISCUSSION

Whereas genetic and genomic studies in *Arabidopsis* (Stone et al., 2005; Vierstra, 2009; Hua and Vierstra, 2011) and comparisons to proteomic studies in other eukaryotes (Peng et al., 2003; Kirkpatrick et al., 2005; Mayor et al., 2005; Tagwerker et al., 2006; Xu et al., 2010; Danielsen et al., 2011; Emanuele et al., 2011; Kim et al., 2011; Wagner et al., 2011) have implied that thousands of ubiquitylation targets exist in plants, prior proteomic studies tentatively identified only a small fraction. This limitation was caused in part by inadequately robust isolation protocols and insufficiently sensitive MS methods to sequence such complex mixtures (Maor et al., 2007; Manzano et al., 2008; Igawa et al., 2009; Saracco et al., 2009). Here, we demonstrate that the application of the TUBEs strategy (Hjerpe et al., 2009) in conjunction with *hexa(6His-UBQ)* plants and Ni-NTA chromatography in a two-step affinity method help overcome these hurdles. The use of TUBEs affinity resins in particular not only provided a more stringent enrichment of ubiquitylated proteins, they also recognized poly-Ub chains with various chain architectures, thus allowing us to generate a more expansive ubiquitylome catalog with presumably less false positives. In fact, we found that harsh conditions could now be used to wash the TUBEs or 2xUSU columns to minimize contaminates that bind the matrices nonspecifically or stay associated noncovalently with the bound conjugates. Further stringency was provided by eliminating proteins also identified in mock purifications, even though some might be ubiquitylated. Such improvements combined with a higher sensitivity mass spectrometer clearly underpin the deeper ubiquitylome reported here and its weak overlap with abundant *Arabidopsis* proteins (MS detectable) that could corrupt the preparations.

The poor overlap of our ubiquitylome catalog with those obtained previously by less stringent single-step methods (7 to 29%; Maor et al., 2007; Manzano et al., 2008; Igawa et al., 2009) as well as the poor overlap among these prior lists by themselves (3 to 14%) calls into question past proteomic studies. While some of this nonoverlap could reflect the different source tissues used in each case (e.g., cell suspension cultures), it also highlights the need for multistep purification approaches for ubiquitylome studies with plants (Saracco et al., 2009; this article). As an aside, our MS-detectable list now provides a reasonably deep view of abundant *Arabidopsis* proteins in whole seedlings that can be applied to other proteomic investigations (see Supplemental Data Set 4 online).

As large as the current ubiquitylome catalog is for green *Arabidopsis* seedlings (941 targets), it is likely biased for abundant cytoplasmic Ub targets and certainly not saturated given our focus on a single developmental stage and the sometimes stochastic nature of MS/MS analysis for low-abundance proteins. Such insufficient coverage is supported by the fact that several well known ubiquitylation targets were not detected here (e.g., auxin/indole-3-acetic acid proteins, EIN3, ABI3, and ABI5), presumably due to their low steady state levels in planta. Consequently, full appreciation might be aided by more focused studies on plants at specific developmental stages or exposed to different environmental conditions, samples probing specific tissue/cell types, and/or fractions enriched in various intracellular compartments. This is supported by our preliminary proteomic analyses of etiolated *Arabidopsis* seedling undergoing photomorphogenesis, which identified a number of ubiquitylated proteins not detected in green seedlings, including phyA, one of the first known targets of the UPS (Shanklin et al., 1987; Jabben et al., 1989).

An obvious emphasis should be on the nuclear fraction given the expected role(s) of Ub and the UPS in controlling the levels/action of various transcriptional regulators and chromatin scaffold proteins (Dreher and Callis, 2007; Vierstra, 2009; Hua and Vierstra, 2011), together with the fact that our MS analysis of whole plants detected so few nuclear components. Others would be various membrane surfaces facing the cytoplasm given the importance of ubiquitylation in protein trafficking and membrane protein turnover (Mukhopadhyay and Riezman, 2007; MacGurn et al., 2012). The presence of a number of H^+-ATPase and aquaporin isoforms in our ubiquitylome catalog suggests a key role for Ub in controlling plasma membrane protein activity and/or turnover, likely via an endocytosis pathway that extracts the receptors from the membrane and delivers them to the vacuole for turnover. This is supported by the report that expression of a fusion between Ub and H^+-ATPase AHA1 in *Arabidopsis* was sufficient to induce its endocytosis and sorting into the vacuolar lumen (Herberth et al., 2012). Deeper coverage might also be possible by using two-step LC methods, such as multidimensional protein identification technology, to further fractionate the peptides before MS analysis (Maor et al., 2007).

From comparisons of our lists generated with TUBEs versus 2xUSU, we also noticed a differential enrichment for specific Ub conjugates, suggesting that an assortment of Ub-binding domains might be necessary to achieve complete coverage of the plant ubiquitylome. In agreement, prior studies using yeast mutants missing various Ub receptors implied that individual Ub-binding domains might be dedicated to specific subsets of conjugates in vivo (Verma et al., 2004; Mayor et al., 2005). To date, 21 different Ub-binding domains have been identified besides UBA, including UIM, UBM, UBZ, ZnF_A20, MUI, CUE, and Pleckstrin homology (Harper and Schulman, 2006; Husnjak and Dikic, 2012), that could be exploited. Whether the affinity of these domains for Ub is sufficient in isolation or could be improved by TUBEs concatenation is not yet known. At present, it is also unclear if the TUBEs matrices will effectively bind ubiquitylated proteins not bearing poly-Ub chains. For both the TUBEs and 2xUSU concatemers, a clear enrichment for poly-Ub chains versus single Ubs was evident at least in vitro. Consequently, additional strategies might be required to enrich for monoubiquitylated targets or targets modified at multiple sites with single Ub moieties.

Based on the current list of ubiquitylated proteins, a number of seminal observations emerge. First, as predicted, ubiquitylation influences a wide range of physiological and developmental processes in plants with a concentration in metabolism and hormone signaling. With the list of targets likely to increase to well over a thousand once greater coverage of the ubiquitylome is achieved, a near one-to-one ratio of E3s to targets is expected in line with the prediction that many of the 1500 *Arabidopsis* E3s are target specific (Vierstra, 2009). Within a number of metabolic and signaling pathways, we identified a collection of ubiquitylated proteins, indicating that this posttranslational modification can be influential at multiple points. This control was particularly evident in the phenylpropanoid biosynthetic pathway, nitrate assimilation, and carbohydrate metabolism and gluconeogenesis. Furthermore, the inclusion of a number of intermediate signaling components, such as MAP kinases (four), calcium-dependent protein kinases (CDPKs) (four), and 14-3-3/GRF proteins (seven of 15 members), also suggests that Ub addition controls the cross-talk between pathways likely via programmed proteolysis.

Second, based on the increased abundance of ubiquitylated targets from plants pretreated with MG132, it is likely that many become substrates of the 26S proteasome. Those targets whose ubiquitylation status did not rise could reflect nonproteolytic outcomes. Alternatively, the emerging connection between ubiquitylation and autophagy, including the discovery that Ub-binding receptors exist that tether ubiquitylated proteins to the enveloping autophagosome (Johansen and Lamark, 2011; Li and Vierstra, 2012), also implies that some might be destined to breakdown via an autophagic route that is immune to proteasome inhibition.

The contrasting effects of MG132 on the ubiquitylation state of the 26S proteasome and the ribosome are particularly intriguing. Increased proteasome ubiquitylation could reflect (1) inadvertent ubiquitylation by E3s bound to the proteasome when the substrate turnover is blocked, (2) a role for the UPS in removing free proteasome subunits that accumulate when proteasome assembly is stalled by MG132, and/or (3) removal of MG132-inactivated particles. In support of the later two scenarios, MG132 exposure also induces a rise in transcripts encoding 26S proteasome subunits and the PA200 and CDC48 alternate caps, presumably to replace misassembled/inactivated complexes (Yang et al., 2004; Book et al., 2009; Book et al., 2010; see Supplemental Figure 7A online). This turnover is likely driven by selective autophagy following proteasome ubiquitylation (Dengjel et al., 2012; Li and Vierstra, 2012).

However, the reason(s) underpinning the lack or inverse effect on ribosomal protein ubiquitylation by MG132 is unclear. MG132 treatment did not significantly alter levels of the *26S* and *18S* rRNAs that scaffold the ribosome nor the mRNAs encoding the representative ribosomal subunits RPS3a (S3), RPS3b (S3), and RPS5a (S5) (see Supplemental Figure 10 online) but strongly reduced the accumulation of the corresponding proteins (Figure 6), implying that the inhibitor does not impact synthesis but might actually accelerate turnover instead of retarding it. An interesting scenario is that proteasomal inhibition sufficiently reduces the pool of free amino acids by interfering with protein

recycling and/or stalls cell division sufficiently, which in turn selectively encourages turnover of existing ribosomes to ultimately reduce translation capacity. This accelerated turnover would presumably occur without a compensatory drop in transcription of the associated RNAs. Ribosomal turnover is known to occur via a selective autophagic process called ribophagy that in yeast surprisingly requires the DUB Ubp3, leading to the hypothesis that deubiquitylation of one or more ribosome subunits is required (Kraft et al., 2008). Ribophagy has recently been observed in plants (Hillwig et al., 2011). The fact that plants encode DUBs related to *Saccharomyces cerevisiae* Ubp3 (UBP3 and UBP24 in *Arabidopsis*; Yan et al., 2000) and our discovery that deubiquitylation might be involved suggest that a similar DUB-directed mechanism occurs in plants as well.

Third, this work expands the collection of Ub attachment sites using the canonical Lys isopeptide linkage, which can now be used to explore the role(s) of this modification in individual proteins by Lys-to-Arg substitutions. As an example, we defined a Ub-linkage site in AGO2, which appears destined for autophagic turnover following ubiquitylation (Gibbings et al., 2012; Derrien et al., 2012). This Lys is conserved in all but one of the AGO paralogs in *Arabidopsis*, suggesting that substituting this residue could influence the turnover of it and other family members. Unfortunately, an alignment of residues surrounding all known Ub-attachment sites in *Arabidopsis* (216 in total) failed to identify one or more consensus Ub-binding motifs. Consequently, our list of ubiquitylation sites does not appear to have predictive value for other proteins not yet linked to ubiquitylation.

Fourth, as in other eukaryotes, *Arabidopsis* and likely other plants assemble an array of poly-Ub chains onto its targets. The strong bias for Lys-48, Lys-63, and Lys-11 internally linked chains compared with others (i.e., Lys-6, Lys-29, and Lys-33) is consistent with previous studies with *Arabidopsis* (Maor et al., 2007; Saracco et al., 2009) and other eukaryotes (Husnjak and Dikic, 2012; Komander and Rape, 2012), but a definitive conclusion about such preferences will require more comprehensive MS analyses with other Ub-binding motifs and other *Arabidopsis* tissues/cell types. The strong shift in chain linkage preference from Lys-48 to Lys-11 upon MG132 treatment suggests that the 26S proteasome favors this linkage in identifying appropriate substrates. This shift could help commit a subpopulation of targets to more rapid proteasomal turnover or enhance the association of all substrates with the core Ub receptors within the proteasome (RPN1, RPN10, and RPN13; Finley, 2009) or its associated shuttle proteins (e.g., the RAD23 family; Farmer et al., 2010). A similar enrichment for Lys-11 chains was seen with yeast encouraged to synthesize abnormal proteins destined to ERAD-dependent UPS turnover (Xu et al., 2009).

Fifth, we emphasize that some of the 941 Ub targets identified here are also altered by other posttranslational modifications, including phosphorylation (PhosPhAt4.0; http://phosphat.mpimp-golm.mpg.de/), Lys acetylation (Finkemeier et al., 2011; Wu et al., 2011), and/or SUMOylation (Miller et al., 2010, 2013) (see Supplemental Data Set 6 online for analysis of our data sets for Lys acetylation and Ser, Thr, and Lys phosphorylation). In total, 330, 15, and 29 of the Ub substrates identified here are affected by one or more of these other modifications, respectively, indicating that *Arabidopsis* encourages a dynamic interplay between these alterations for protein regulation. The strong overlap with phosphorylation (35% of Ub substrates) is consistent with the crucial importance of this modification in driving target recognition by specific E3s (Vierstra, 2009). Conversely, because acetylation and ubiquitylation compete for Lys residues, antagonistic roles are possible (Danielsen et al., 2011; Wagner et al., 2011). Examples of multiply modified proteins include nitrate reductase, which is ubiquitylated (this article), phosphorylated (Lambeck et al., 2012), and SUMOylated (Park et al., 2011), and the AHA H^+-ATPases that are regulated by phosphorylation and possibly ubiquitylation (Palmgren, 2001; this article). Intriguingly, we mapped a site for Ub addition on AHA2 to a strictly conserved Lys (Lys-300) close to the phosphorylation site (Asp-329) that regulates its activity and its potential interaction with the 14-3-3/GRF proteins GRF2 and GRF4 (Baunsgaard et al., 1998), which are themselves likely ubiquitylation targets. For SUMOylation, we recently observed that some targets become ubiquitylated during stress following SUMOylation with the SUMO moiety predicted to not only provide the recognition domain for SUMO-dependent Ub E3s but also the site(s) for Ub attachment (Miller et al., 2010, 2013).

In conclusion, our improved methods to isolate Ub conjugates from *Arabidopsis* now offer a richer picture of this posttranslational modification and how it might impact plant growth and development. Through the analysis of this conjugation for individual substrates, especially those for which the exact binding sites have been mapped, it should be possible to define how ubiquitylation specifically affects their activity and/or turnover. Given that the TUBEs matrices described here are universally applicable, a facile strategy is now available to characterize the ubiquitylome in any plant species.

METHODS

Preparation of TUBEs and 2xUSU Affinity Matrices

The USU construction encoding residues 158 to 357 of human HHR23A (Raasi et al., 2004) fused to the C terminus of GST in the pGEX-4T plasmid was as described (Saracco et al., 2009). The 2xUSU coding region was assembled by connecting the nucleotides encoding two USU domains in frame with an oligonucleotide encoding the GGGGSGGGGS linker. For the TUBEs construction, the region encoding the UBA1 domain from HHR23A (residues 158 to 212) was connected back-to-back four times and linked by oligonucleotides encoding the GGGSGGG sequence. Both the 2xUSU and TUBEs constructions were appended in frame to the 3′ end of the GST coding region upon introduction into the *Bam*HI and *Xho*I sites of the pGEX-4T plasmid. The GST alone protein control was encoded in the unmodified pGEX-4T plasmid.

The GST-USU, GST-2xUSU, GST-TUBEs, and GST proteins were expressed in BL21 pLysS *Escherichia coli* following a 4-h induction with 1 mM isopropyl-β-D-thiogalactopyranoside and affinity purified with the GST-Bind Resin (EMD4 Biosciences). Purified GST and GST fusion proteins were dialyzed overnight against 50 mM MOPS, pH 7.5, and concentrated using an Ultracel-10K filter (Millipore). The proteins were coupled to AffiGel-15 beads (Bio-Rad) overnight at 4°C at a concentration of 5 mg/mL of beads. The decorated beads were incubated with 100 mM Tris-HCl, pH 7.5, for 1 h on ice to quench the reaction, washed with 10 volumes of MOPS-KOH, pH 7.5, followed by 10 volumes of protein extraction buffer (EB; 50 mM Tris-HCl, pH 7.2, 200 mM NaCl, and 0.25% Triton X-100), and then stored at 4°C in EB until use.

In Vitro Ub Chain Binding Assays

The GST, GST-USU, GST-2xUSU, and GST-TUBEs proteins were immobilized on prewashed GST-Bind Resin in binding buffer (BB; 50 mM Tris-HCl, pH 7.5, 100 mM NaCl, 1 mM Na_2EDTA, and 0.1% Nonidet P-40). Twenty micrograms of each protein was incubated at 4°C for 1 h with 5 μg of purified Lys-11–linked chains (Ub_2+Ub_4) or a mixture of Lys-48– or Lys-63–linked poly-Ub chains (Ub_{2-7}) (Boston Biochem) in BB and then washed extensively in ice-cold BB. Bound conjugates were released by heating the beads in SDS-PAGE sample buffer and then detected by immunoblot analysis of the supernatants with anti-Ub antibodies following SDS-PAGE (Farmer et al., 2010). Signals were detected with Classic Autoradiography Film (MIDSCI), with exposure times kept within the linear range of the film. Relative binding was quantified from densitometric scans of the films with Image J (http://rsp.info.nih.gov.ij) using the signals generated by dilution series of the input poly-Ub chains as standards. Binding efficiencies of 2xUSU and TUBEs compared with USU were normalized using the molecular mass ratio of the each protein versus USU (1.38- and 1.04-fold, respectively).

Affinity Purification of Ub-Protein Conjugates

Seeds of *Arabidopsis thaliana* ecotype Col-0 wild type and homozygous for the *hexa(6His-UBQ)* transgene (Saracco et al., 2009) were surface sterilized, stratified in the dark at 4°C for 3 d, and then germinated in liquid Gamborg's B5 minimal medium (Sigma-Aldrich) containing 2% Suc with the pH of the medium adjusted to 5.7 using KOH. The cultures were grown for 10 d with slow shaking (90 rpm) at 26°C under continuous white light. MG132 (carbobenzoxyl-Leu-Leu-Leu-al; Enzo Life Sciences) dissolved in DMSO was added at a final concentration of 50 μM to the cultures 12 h before harvest. Seedlings (~50 g) were collected, blotted dry, rapidly frozen in liquid nitrogen, and then stored at −80°C until use. Frozen tissue was powdered at liquid nitrogen temperatures and then mixed with 0.5 g/mL EB containing 0.25% Triton X-100, 1× protease inhibitor cocktail (Roche), 2 mM phenylmethanesulfonyl fluoride, 10 mM 2-chloroacetamide, 10 mM sodium metasulfite, and 1 mM *N*-ethylmaleimide added just before use. The homogenate was filtered through two layers of Miracloth and one layer of cheesecloth and clarified at 12,000*g* for 20 min. This supernatant was analyzed by LC-MS/MS directly following trypsinization and is referred to here as the MS-detectable fraction.

Homogenates equivalent to 40 g of tissue were mixed with 1 mL of GST-, GST-2xUSU-, or GST-TUBEs–decorated beads and incubated for 6 h at 4°C with gentle shaking. Beads were collected in a 2 × 1-cm chromatography column and washed three times with EB and three times with EB plus 2 M NaCl. The bound proteins were eluted at room temperature in 10 mL of 7 M guanidine-HCl, 100 mM NaH_2PO_4, and 10 mM Tris-HCl, pH 8.0. The eluates were supplemented with 20 mM imidazole and 10 mM 2-chloroacetamide and incubated for 12 h at 4°C with 500 μL of Ni-NTA agarose (Qiagen) preequilibrated in the same buffer. The beads were collected in a 1.5 × 1-cm chromatography column and washed once in 6 M guanidine-HCl, 0.1% SDS, 100 mM NaH_2PO_4, and 10 mM Tris-HCl, pH 8.0, and once in urea buffer (UB; 8 M urea, 100 mM NaH_2PO_4, and 10 mM Tris-HCl, pH 8.0) plus 0.1% Triton X-100, twice in UB plus 20 mM imidazole, and three times in UB alone. Bound proteins were eluted in UB plus 400 mM imidazole. Eluted proteins were pooled and concentrated using an Ultracel-10K filter (Millipore). The purity of the preparations was assessed after SDS-PAGE by staining for total protein with silver and by immunoblot analysis with anti-Ub (Shanklin et al., 1987) or anti-5His antibodies (Novagen). Anti-PBA1 (Book et al., 2010) and anti-histone H3 antibodies (Abcam) were used to confirm near equal protein loading.

To demonstrate that the purification conditions were sufficiently harsh to denature protein/protein complexes, pull-down assays for the 26S proteasome complex were performed with extracts from 10-d-old green *PAG1-Flag pag1-1* seedlings prepared with or without treatment with denaturants (Book et al., 2010). Crude extracts were generated with EB and protease inhibitors as above, clarified, either left alone (Native) or supplemented with 8 M urea or 7 M guanidine-HCl by adding the crystalline chemicals directly, and incubated for 20 min with gentle shaking at ice temperatures. The solutions were dialyzed for 16 h against 25 mM Tris-HCl, pH 7.2, at 4°C and then applied to an anti-Flag M2 affinity column (Sigma-Aldrich). After three washes with EB, the bound proteins were eluted with the Flag epitope peptide (Book et al., 2010). To further stabilize the association of the RP and CP subcomplexes with ATP, crude extracts were prepared with buffer A [50 mM 4-(2-hydroxyethyl)-1-piperazineethanesulfonic acid, pH 7.5, 25 mM NaCl, 2 mM $MgCl_2$, 1 mM EDTA, 5% (v/v) glycerol, and 10 mM ATP], and 2 mM phenylmethylsulfonyl fluoride added just before use, clarified, and either left alone (Native) or brought to 8 M urea as above. After a 20-min incubation on ice, the samples were diluted 10-fold in buffer A and applied to the anti-Flag affinity column. After three washes with buffer A, bound proteins were eluted with buffer A plus the Flag peptide. Eluted proteins from both conditions (±ATP) were subjected to SDS-PAGE and immunoblot analyses with antibodies that recognize the proteasome subunits PBA1, RPN1a, RPN5a, RPT2a, and RPT4b (Smalle et al., 2003; Book et al., 2010; Lee et al., 2011).

MS

Control and ubiquitylated protein mixtures (100 μL) were carbamidomethylated in the dark for 1 h by reduction with 10 mM DTT, followed by alkylation with 30 mM 2-chloroacetamide for 1 h (Nielsen et al., 2008); the reaction was quenched by incubation with 20 μL of 200 mM DTT for 10 min. Samples were diluted 10-fold with 25 mM ammonium bicarbonate and incubated at 37°C for 12 h with 2 μg of sequencing grade trypsin (Promega) followed by a second 6-h incubation with an additional 2 μg of trypsin. The tryptic digests were desalted using a C18 solid-phase extraction pipette tip (SPEC PT C18; Varian), vacuum-dried, and reconstituted in 10 μL of 95% water, 5% acetonitrile, and 0.1% formic acid.

Samples were analyzed by electrospray ionization MS using a system consisting of a nanoflow liquid chromatograph (nanoAcquity; Waters) connected online to an electrospray ionization FT/ion-trap mass spectrometer (LTQ orbitrap Velos; ThermoFisher Scientific). LC separation employed a 100 × 365 -μm fused silica capillary microcolumn packed with 15 cm of 3-μm-diameter, 100-Å pore size, C18 beads (Magic C18; Bruker), with the emitter tip pulled to ~2 μm using a laser puller (Sutter Instruments). Peptides were loaded on the column at a flow rate of 500 nL/min for 30 min and then eluted over 120 min at a flow rate of 200 nL/min with a gradient of 2 to 30% acetonitrile in 0.1% formic acid. Full mass scans were performed in the FT orbitrap between 300 and 1500 mass-to-charge ratio at a resolution of 60,000, followed by 10 MS/MS HCD scans of the 10 highest intensity parent ions at 42% relative collision energy and 7500 resolution, with a mass range starting at 100 mass-to-charge ratio. Dynamic exclusion was enabled with a repeat count of two over the duration of 30 s and an exclusion window of 120 s.

MS Data Analysis

The acquired precursor MS and MS/MS spectra were searched against the *Arabidopsis* ecotype Col-0 protein database (IPI database, version 3.85 containing 39,677 entries; The Arabidopsis Information Resource [TAIR], http://www.Arabidopsis.org) using SEQUEST version 1.2 (ThermoFisher Scientific). All raw spectra are available in the Peptide Atlas Database (http://www.peptideatlas.org/PASS/PASS00229). Masses for both precursor and fragment ions were treated as monoisotopic. Oxidized Met (+15.995 D), carbamidomethylated Cys residues (+57.021 D), and the di-Gly Ub footprint (+114.043 D) attached to Lys residues were allowed as dynamic modifications. The database search allowed for up to two missed trypsin cleavages, and ion masses were matched with a mass tolerance of

10 ppm for precursor masses and 0.1 D for HCD fragments. The data were filtered using a 1% FDR (Rohrbough et al., 2006), with a minimum of two peptide matches required for confident protein identification. In total, the MS analyses identified 19,130 peptides that could be assigned to 941 individual ubiquitylated proteins following subtraction of contaminants. The data sets were also screened for Lys acetylation (+42.011 D) and phosphorylation at Ser, Thr, or Lys residues (+79.966 D) by SEQUEST using a 5% FDR for single matching peptides (see Supplemental Data Set 6 online). Attempts to identify a consensus Ub attachment site by IceLogo (Colaert et al., 2009) incorporated the six amino acids N- and C-terminal to the modified Lys for 216 Ub footprint sites identified from the *Arabidopsis* Ub proteomics studies of Maor et al. (2007), Saracco et al. (2009), Book et al. (2010), and this article. The GO annotations for the Ub targets (941 proteins) and the complete *Arabidopsis* proteome (27,430 proteins) were determined by hand analysis using MIPS-FunCat (Ruepp et al., 2004). The SUBA3 database was used for the predicting subcellular localization of proteins (Tanz et al., 2013).

Effects of MG132

The response of 26S proteasome and ribosomal subunits to MG132 was determined by immunoblot analysis with antibodies against *Arabidopsis* proteasome subunits, the proteasome accessory proteins PA200 (Book et al., 2010) and CDC48 (Park et al., 2007), and the human ribosome subunits RPS3 (Abcam ab77772) and RPS2 (Aviva Systems Biology; ARP63572_P050), the latter of which is orthologous to *Arabidopsis* RPS5. The anti-RPS3 antibodies were generated against the middle region of human RPS3 (residues ~50 to 150), which is 88% identical between human and *Arabidopsis* RPS3 (At2g31610 and At5g35530). Antibodies against histone H3 (Abcam ab1791) were used to confirm equal protein loading. rRNA levels in MG132-treated seedlings were determined by RNA gel blot analysis of total RNA extracted from 10-d-old seedlings by the TRIzol method (Rio et al., 2010). mRNA levels for several proteasome and ribosome subunit genes were assessed semiquantitatively by RT-PCR using gene-specific primers and total RNA templates isolated from 10-d-old liquid-grown green seedlings (±MG132).

Accession Numbers

Accession numbers to all *Arabidopsis* proteins identified in this study in accordance with the TAIR database can be found in Supplemental Data Sets 1 to 5 online. All raw MS spectra are available in the Peptide Atlas Database (http://www.peptideatlas.org/PASS/PASS00229).

Supplemental Data

The following materials are available in the online version of this article.

Supplemental Figure 1. Purification Efficiency of Ub-Binding Domains for *Arabidopsis* Proteins Ubiquitylated in Vivo.

Supplemental Figure 2. Inhibition of Ub Conjugate Disassembly/Degradation by Protease Inhibitors.

Supplemental Figure 3. Enrichment of Ub Conjugates from a Transgenic *Arabidopsis* Line Expressing 6His-Ub.

Supplemental Figure 4. Overlap of *Arabidopsis* Proteins Identified by MS in Three Biological Replicates.

Supplemental Figure 5. Effect of MG132 on Ub Conjugate Levels and the Proteolytic Maturation of the 26S Proteasome β1 Subunit PBA1.

Supplemental Figure 6. Correlation between Fold Change of Ub Conjugates ±MG132 and Their Abundance Estimated by PSMs.

Supplemental Figure 7. Involvement of Ubiquitylation in the Phenylpropanoid Biosynthetic Pathway.

Supplemental Figure 8. Dissociation of the 26S Proteasome Complex by Urea or Guanidine-HCl.

Supplemental Figure 9. Analysis of the Amino Acid Sequences Surrounding Ub-Attachment Sites.

Supplemental Figure 10. RT-PCR and RNA Gel Analysis of Proteasome- and Ribosome-Associated Genes in Seedlings Treated ±MG132.

Supplemental Data Set 1. List of Contaminant Proteins Identified by MS.

Supplemental Data Set 2. Complete List of *Arabidopsis* Ub Conjugates Identified by MS.

Supplemental Data Set 3. List of Top Five Most Abundant Ubiquitylated Proteins Based on PSMs in Each of the 10 Functional GO Categories for *Arabidopsis*.

Supplemental Data Set 4. List of MS-Detectable *Arabidopsis* Proteins Identified by Direct MS Analysis of Trypsinized Crude Seedling Extracts.

Supplemental Data Set 5. Complete List of Known Ub Footprint Peptides in *Arabidopsis*.

Supplemental Data Set 6. List of *Arabidopsis* Proteins Found in Our MS/MS Data Sets That Are Modified by Lys Acetylation or Phosphorylation at Ser, Thr, and/or Lys Residues.

ACKNOWLEDGMENTS

We thank Scott A. Sarraco, Marcus M. Miller, David C. Gemperline, Nicholas J. Gladman, and Joseph M. Walker for materials and technical advice. We also thank Sebastian Y. Bednarek for kindly providing anti-CDC48 antibodies. This work was supported by a National Science Foundation *Arabidopsis* 2010 Program grant (MCB-0929100) to R.D.V. and grants from National Institutes of Health/National Human Genome Research Institute (1P50HG004952) and National Institutes of Health/National Institute of General Medical Sciences (P01GM081629) to M.S. and L.M.S.

AUTHOR CONTRIBUTIONS

D.-Y.K. and R.D.V. designed the research, analyzed the data, and wrote the article. D.-Y.K. developed the purification strategy and conducted the protein isolations. M.S. performed the MS analyses and helped with protein identification. M.S. and L.M.S. developed the MS pipeline.

Received December 18, 2012; revised April 11, 2013; accepted April 18, 2013; published May 10, 2013.

REFERENCES

Baunsgaard, L., Fuglsang, A.T., Jahn, T., Korthout, H.A., de Boer, A.H., and Palmgren, M.G. (1998). The 14-3-3 proteins associate with the plant plasma membrane H(+)-ATPase to generate a fusicoccin binding complex and a fusicoccin responsive system. Plant J. **13:** 661–671.

Book, A.J., Gladman, N.P., Lee, S.S., Scalf, M., Smith, L.M., and Vierstra, R.D. (2010). Affinity purification of the *Arabidopsis* 26S proteasome reveals a diverse array of plant proteolytic complexes. J. Biol. Chem. **285:** 25554–25569.

Book, A.J., Smalle, J., Lee, K.H., Yang, P., Walker, J.M., Casper, S., Holmes, J.H., Russo, L.A., Buzzinotti, Z.W., Jenik, P.D., and Vierstra, R.D. (2009). The RPN5 subunit of the 26S proteasome is essential for gametogenesis, sporophyte development, and complex assembly in *Arabidopsis*. Plant Cell **21:** 460–478.

Chevalier, D., and Walker, J.C. (2005). Functional genomics of protein kinases in plants. Brief. Funct. Genomics Proteomics **3:** 362–371.

Colaert, N., Helsens, K., Martens, L., Vandekerckhove, J., and Gevaert, K. (2009). Improved visualization of protein consensus sequences by iceLogo. Nat. Methods **6:** 786–787.

Danielsen, J.M., Sylvestersen, K.B., Bekker-Jensen, S., Szklarczyk, D., Poulsen, J.W., Horn, H., Jensen, L.J., Mailand, N., and Nielsen, M.L. (2011). Mass spectrometric analysis of lysine ubiquitylation reveals promiscuity at site level. Mol. Cell. Proteomics **10:** M110.003590.

Dengjel, J., et al. (2012). Identification of autophagosome-associated proteins and regulators by quantitative proteomic analysis and genetic screens. Mol. Cell. Proteomics **11:** M111.014035.

Derrien, B., Baumberger, N., Schepetilnikov, M., Viotti, C., De Cillia, J., Ziegler-Graff, V., Isono, E., Schumacher, K., and Genschik, P. (2012). Degradation of the antiviral component ARGONAUTE1 by the autophagy pathway. Proc. Natl. Acad. Sci. USA **109:** 15942–15946.

Dreher, K., and Callis, J. (2007). Ubiquitin, hormones and biotic stress in plants. Ann. Bot. (Lond.) **99:** 787–822.

Ellgaard, L., and Helenius, A. (2003). Quality control in the endoplasmic reticulum. Nat. Rev. Mol. Cell Biol. **4:** 181–191.

Emanuele, M.J., Elia, A.E., Xu, Q., Thoma, C.R., Izhar, L., Leng, Y., Guo, A., Chen, Y.N., Rush, J., Hsu, P.W., Yen, H.C., and Elledge, S.J. (2011). Global identification of modular cullin-RING ligase substrates. Cell **147:** 459–474.

Farmer, L.M., Book, A.J., Lee, K.H., Lin, Y.L., Fu, H., and Vierstra, R.D. (2010). The RAD23 family provides an essential connection between the 26S proteasome and ubiquitylated proteins in *Arabidopsis*. Plant Cell **22:** 124–142.

Finkemeier, I., Laxa, M., Miguet, L., Howden, A.J., and Sweetlove, L.J. (2011). Proteins of diverse function and subcellular location are lysine acetylated in *Arabidopsis*. Plant Physiol. **155:** 1779–1790.

Finley, D. (2009). Recognition and processing of ubiquitin-protein conjugates by the proteasome. Annu. Rev. Biochem. **78:** 477–513.

Gibbings, D., Mostowy, S., Jay, F., Schwab, Y., Cossart, P., and Voinnet, O. (2012). Selective autophagy degrades DICER and AGO2 and regulates miRNA activity. Nat. Cell Biol. **14:** 1314–1321.

Harper, J.W., and Schulman, B.A. (2006). Structural complexity in ubiquitin recognition. Cell **124:** 1133–1136.

Herberth, S., Shahriari, M., Bruderek, M., Hessner, F., Müller, B., Hülskamp, M., and Schellmann, S. (2012). Artificial ubiquitylation is sufficient for sorting of a plasma membrane ATPase to the vacuolar lumen of *Arabidopsis* cells. Planta **236:** 63–77.

Hillwig, M.S., Contento, A.L., Meyer, A., Ebany, D., Bassham, D.C., and Macintosh, G.C. (2011). RNS2, a conserved member of the RNase T2 family, is necessary for ribosomal RNA decay in plants. Proc. Natl. Acad. Sci. USA **108:** 1093–1098.

Hjerpe, R., Aillet, F., Lopitz-Otsoa, F., Lang, V., England, P., and Rodriguez, M.S. (2009). Efficient protection and isolation of ubiquitylated proteins using tandem ubiquitin-binding entities. EMBO Rep. **10:** 1250–1258.

Hua, Z., and Vierstra, R.D. (2011). The cullin-RING ubiquitin-protein ligases. Annu. Rev. Plant Biol. **62:** 299–334.

Hua, Z., Zou, C., Shiu, S.H., and Vierstra, R.D. (2011). Phylogenetic comparison of F-Box (FBX) gene superfamily within the plant kingdom reveals divergent evolutionary histories indicative of genomic drift. PLoS ONE **6:** e16219.

Husnjak, K., and Dikic, I. (2012). Ubiquitin-binding proteins: Decoders of ubiquitin-mediated cellular functions. Annu. Rev. Biochem. **81:** 291–322.

Igawa, T., Fujiwara, M., Takahashi, H., Sawasaki, T., Endo, Y., Seki, M., Shinozaki, K., Fukao, Y., and Yanagawa, Y. (2009). Isolation and identification of ubiquitin-related proteins from *Arabidopsis* seedlings. J. Exp. Bot. **60:** 3067–3073.

Iwai, K., and Tokunaga, F. (2009). Linear polyubiquitination: A new regulator of NF-kappaB activation. EMBO Rep. **10:** 706–713.

Jabben, M., Shanklin, J., and Vierstra, R.D. (1989). Ubiquitin-phytochrome conjugates. Pool dynamics during in vivo phytochrome degradation. J. Biol. Chem. **264:** 4998–5005.

Jin, L., Williamson, A., Banerjee, S., Philipp, I., and Rape, M. (2008). Mechanism of ubiquitin-chain formation by the human anaphase-promoting complex. Cell **133:** 653–665.

Johansen, T., and Lamark, T. (2011). Selective autophagy mediated by autophagic adapter proteins. Autophagy **7:** 279–296.

Kim, W., Bennett, E.J., Huttlin, E.L., Guo, A., Li, J., Possemato, A., Sowa, M.E., Rad, R., Rush, J., Comb, M.J., Harper, J.W., and Gygi, S.P. (2011). Systematic and quantitative assessment of the ubiquitin-modified proteome. Mol. Cell **44:** 325–340.

Kirkpatrick, D.S., Weldon, S.F., Tsaprailis, G., Liebler, D.C., and Gandolfi, A.J. (2005). Proteomic identification of ubiquitinated proteins from human cells expressing His-tagged ubiquitin. Proteomics **5:** 2104–2111.

Komander, D., and Rape, M. (2012). The ubiquitin code. Annu. Rev. Biochem. **81:** 203–229.

Kraft, C., Deplazes, A., Sohrmann, M., and Peter, M. (2008). Mature ribosomes are selectively degraded upon starvation by an autophagy pathway requiring the Ubp3p/Bre5p ubiquitin protease. Nat. Cell Biol. **10:** 602–610.

Kwon, S.J., Choi, E.Y., Choi, Y.J., Ahn, J.H., and Park, O.K. (2006). Proteomics studies of post-translational modifications in plants. J. Exp. Bot. **57:** 1547–1551.

Lambeck, I.C., Fischer-Schrader, K., Niks, D., Roeper, J., Chi, J.C., Hille, R., and Schwarz, G. (2012). Molecular mechanism of 14-3-3 protein-mediated inhibition of plant nitrate reductase. J. Biol. Chem. **287:** 4562–4571.

Lee, K.H., Minami, A., Marshall, R.S., Book, A.J., Farmer, L.M., Walker, J.M., and Vierstra, R.D. (2011). The RPT2 subunit of the 26S proteasome directs complex assembly, histone dynamics, and gametophyte and sporophyte development in *Arabidopsis*. Plant Cell **23:** 4298–4317.

Lee, S., Lee, D.W., Lee, Y., Mayer, U., Stierhof, Y.D., Lee, S., Jürgens, G., and Hwang, I. (2009). Heat shock protein cognate 70-4 and an E3 ubiquitin ligase, CHIP, mediate plastid-destined precursor degradation through the ubiquitin-26S proteasome system in *Arabidopsis*. Plant Cell **21:** 3984–4001.

Li, F., and Vierstra, R.D. (2012). Autophagy: A multifaceted intracellular system for bulk and selective recycling. Trends Plant Sci. **17:** 526–537.

Ling, Q., Huang, W., Baldwin, A., and Jarvis, P. (2012). Chloroplast biogenesis is regulated by direct action of the ubiquitin-proteasome system. Science **338:** 655–659.

Lopitz-Otsoa, F., Rodríguez, M.S., and Aillet, F. (2010). Properties of natural and artificial proteins displaying multiple ubiquitin-binding domains. Biochem. Soc. Trans. **38:** 40–45.

MacGurn, J.A., Hsu, P.C., and Emr, S.D. (2012). Ubiquitin and membrane protein turnover: From cradle to grave. Annu. Rev. Biochem. **81:** 231–259.

Manzano, C., Abraham, Z., López-Torrejón, G., and Del Pozo, J.C. (2008). Identification of ubiquitinated proteins in *Arabidopsis*. Plant Mol. Biol. **68:** 145–158.

Maor, R., Jones, A., Nühse, T.S., Studholme, D.J., Peck, S.C., and Shirasu, K. (2007). Multidimensional protein identification technology (MudPIT) analysis of ubiquitinated proteins in plants. Mol. Cell. Proteomics **6:** 601–610.

Mayor, T., Lipford, J.R., Graumann, J., Smith, G.T., and Deshaies, R.J. (2005). Analysis of polyubiquitin conjugates reveals that the Rpn10 substrate receptor contributes to the turnover of multiple proteasome targets. Mol. Cell. Proteomics **4:** 741–751.

Miller, M.J., Barrett-Wilt, G.A., Hua, Z., and Vierstra, R.D. (2010). Proteomic analyses identify a diverse array of nuclear processes affected by small ubiquitin-like modifier conjugation in *Arabidopsis*. Proc. Natl. Acad. Sci. USA **107:** 16512–16517.

Miller, M.J., Scalf, M., Rytz, T.C., Hubler, S.L., Smith, L.M., and Vierstra, R.D. (2013). Quantitative proteomics reveals factors regulating RNA biology as dynamic targets of stress-induced SUMOylation in *Arabidopsis*. Mol. Cell. Proteomics **12:** 449–463.

Mukhopadhyay, D., and Riezman, H. (2007). Proteasome-independent functions of ubiquitin in endocytosis and signaling. Science **315:** 201–205.

Nielsen, M.L., Vermeulen, M., Bonaldi, T., Cox, J., Moroder, L., and Mann, M. (2008). Iodoacetamide-induced artifact mimics ubiquitination in mass spectrometry. Nat. Methods **5:** 459–460.

Okumoto, K., Misono, S., Miyata, N., Matsumoto, Y., Mukai, S., and Fujiki, Y. (2011). Cysteine ubiquitination of PTS1 receptor Pex5p regulates Pex5p recycling. Traffic **12:** 1067–1083.

Palmgren, M.G. (2001). Plant plasma membrane H+-ATPases: Powerhouses for nutrient uptake. Annu. Rev. Plant Physiol. Plant Mol. Biol. **52:** 817–845.

Park, B.S., Song, J.T., and Seo, H.S. (2011). *Arabidopsis* nitrate reductase activity is stimulated by the E3 SUMO ligase AtSIZ1. Nat. Commun. **2:** 400.

Park, S., Rancour, D.M., and Bednarek, S.Y. (2007). Protein domain-domain interactions and requirements for the negative regulation of *Arabidopsis* CDC48/p97 by the plant ubiquitin regulatory X (UBX) domain-containing protein, PUX1. J. Biol. Chem. **282:** 5217–5224.

Peng, J., Schwartz, D., Elias, J.E., Thoreen, C.C., Cheng, D., Marsischky, G., Roelofs, J., Finley, D., and Gygi, S.P. (2003). A proteomics approach to understanding protein ubiquitination. Nat. Biotechnol. **21:** 921–926.

Raasi, S., Orlov, I., Fleming, K.G., and Pickart, C.M. (2004). Binding of polyubiquitin chains to ubiquitin-associated (UBA) domains of HHR23A. J. Mol. Biol. **341:** 1367–1379.

Rio, D.C., Ares, M., Jr., Hannon, G.J., and Nilsen, T.W. (2010). Purification of RNA using TRIzol (TRI reagent). Cold Spring Harb. Protoc. **2010:** pdb prot5439.

Rohrbough, J.G., Breci, L., Merchant, N., Miller, S., and Haynes, P.A. (2006). Verification of single-peptide protein identifications by the application of complementary database search algorithms. J. Biomol. Tech. **17:** 327–332.

Ruepp, A., Zollner, A., Maier, D., Albermann, K., Hani, J., Mokrejs, M., Tetko, I., Güldener, U., Mannhaupt, G., Münsterkötter, M., and Mewes, H.W. (2004). The FunCat, a functional annotation scheme for systematic classification of proteins from whole genomes. Nucleic Acids Res. **32:** 5539–5545.

Santner, A., and Estelle, M. (2010). The ubiquitin-proteasome system regulates plant hormone signaling. Plant J. **61:** 1029–1040.

Saracco, S.A., Hansson, M., Scalf, M., Walker, J.M., Smith, L.M., and Vierstra, R.D. (2009). Tandem affinity purification and mass spectrometric analysis of ubiquitylated proteins in *Arabidopsis*. Plant J. **59:** 344–358.

Shanklin, J., Jabben, M., and Vierstra, R.D. (1987). Red light-induced formation of ubiquitin-phytochrome conjugates: Identification of possible intermediates of phytochrome degradation. Proc. Natl. Acad. Sci. USA **84:** 359–363.

Shen, G., Adam, Z., and Zhang, H. (2007). The E3 ligase AtCHIP ubiquitylates FtsH1, a component of the chloroplast FtsH protease, and affects protein degradation in chloroplasts. Plant J. **52:** 309–321.

Shimizu, Y., Okuda-Shimizu, Y., and Hendershot, L.M. (2010). Ubiquitylation of an ERAD substrate occurs on multiple types of amino acids. Mol. Cell **40:** 917–926.

Smalle, J., Kurepa, J., Yang, P., Emborg, T.J., Babiychuk, E., Kushnir, S., and Vierstra, R.D. (2003). The pleiotropic role of the 26S proteasome subunit RPN10 in *Arabidopsis* growth and development supports a substrate-specific function in abscisic acid signaling. Plant Cell **15:** 965–980.

Smalle, J., and Vierstra, R.D. (2004). The ubiquitin 26S proteasome proteolytic pathway. Annu. Rev. Plant Biol. **55:** 555–590.

Stone, S.L., Hauksdóttir, H., Troy, A., Herschleb, J., Kraft, E., and Callis, J. (2005). Functional analysis of the RING-type ubiquitin ligase family of *Arabidopsis*. Plant Physiol. **137:** 13–30.

Szklarczyk, D., Franceschini, A., Kuhn, M., Simonovic, M., Roth, A., Minguez, P., Doerks, T., Stark, M., Muller, J., Bork, P., Jensen, L.J., and von Mering, C. (2011). The STRING database in 2011: Functional interaction networks of proteins, globally integrated and scored. Nucleic Acids Res. **39:** D561–D568.

Tagwerker, C., Flick, K., Cui, M., Guerrero, C., Dou, Y., Auer, B., Baldi, P., Huang, L., and Kaiser, P. (2006). A tandem affinity tag for two-step purification under fully denaturing conditions: Application in ubiquitin profiling and protein complex identification combined with in vivo cross-linking. Mol. Cell. Proteomics **5:** 737–748.

Tanz, S.K., Castleden, I., Hooper, C.M., Vacher, M., Small, I., and Millar, H.A. (2013). SUBA3: A database for integrating experimentation and prediction to define the SUBcellular location of proteins in *Arabidopsis*. Nucleic Acids Res. **41: D**1185–D1191.

Uhrig, R.G., She, Y.M., Leach, C.A., and Plaxton, W.C. (2008). Regulatory monoubiquitination of phosphoenolpyruvate carboxylase in germinating castor oil seeds. J. Biol. Chem. **283:** 29650–29657.

Verma, R., Oania, R., Graumann, J., and Deshaies, R.J. (2004). Multiubiquitin chain receptors define a layer of substrate selectivity in the ubiquitin-proteasome system. Cell **118:** 99–110.

Vierstra, R.D. (2009). The ubiquitin-26S proteasome system at the nexus of plant biology. Nat. Rev. Mol. Cell Biol. **10:** 385–397.

Vierstra, R.D., and Sullivan, M.L. (1988). Hemin inhibits ubiquitin-dependent proteolysis in both a higher plant and yeast. Biochemistry **27:** 3290–3295.

Vijay-Kumar, S., Bugg, C.E., Wilkinson, K.D., Vierstra, R.D., Hatfield, P.M., and Cook, W.J. (1987). Comparison of the three-dimensional structures of human, yeast, and oat ubiquitin. J. Biol. Chem. **262:** 6396–6399.

Wagner, S.A., Beli, P., Weinert, B.T., Nielsen, M.L., Cox, J., Mann, M., and Choudhary, C. (2011). A proteome-wide, quantitative survey of in vivo ubiquitylation sites reveals widespread regulatory roles. Mol. Cell. Proteomics **10:** M111.013284.

Wu, X., Oh, M.H., Schwarz, E.M., Larue, C.T., Sivaguru, M., Imai, B.S., Yau, P.M., Ort, D.R., and Huber, S.C. (2011). Lysine acetylation is a widespread protein modification for diverse proteins in *Arabidopsis*. Plant Physiol. **155:** 1769–1778.

Xu, G., Paige, J.S., and Jaffrey, S.R. (2010). Global analysis of lysine ubiquitination by ubiquitin remnant immunoaffinity profiling. Nat. Biotechnol. **28:** 868–873.

Xu, P., Duong, D.M., Seyfried, N.T., Cheng, D., Xie, Y., Robert, J., Rush, J., Hochstrasser, M., Finley, D., and Peng, J. (2009). Quantitative proteomics reveals the function of unconventional ubiquitin chains in proteasomal degradation. Cell **137:** 133–145.

Yan, N., Doelling, J.H., Falbel, T.G., Durski, A.M., and Vierstra, R.D. (2000). The ubiquitin-specific protease family from *Arabidopsis*. AtUBP1 and 2 are required for the resistance to the amino acid analog canavanine. Plant Physiol. **124:** 1828–1843.

Yang, P., Fu, H., Walker, J., Papa, C.M., Smalle, J., Ju, Y.M., and Vierstra, R.D. (2004). Purification of the *Arabidopsis* 26S proteasome: Biochemical and molecular analyses revealed the presence of multiple isoforms. J. Biol. Chem. **279:** 6401–6413.